Nat Hazards (2017) 87:255–286
DOI 10.1007/s11069-017-2762-1

ORIGINAL PAPER

Devastating extreme Mediterranean cyclone's impacts in Turkey

Sevinc A. Sirdas[1] · E. Tuncay Özdemir[1,2] · İsmail Sezen[1,2] · Bahtiyar Efe[1] · Vinay Kumar[3]

Received: 26 April 2016 / Accepted: 19 January 2017 / Published online: 17 February 2017

Abstract A tropical cyclone was formed over central northern Africa near Egypt, Libya and Crete, and it moved and deepened toward the north–northeast; meanwhile, the storm destroyed many regions in the west, southwest and central of Turkey. The cyclone carried huge dust from the north of Africa to Turkey and reduced the visibility to less than 1 km and raised the wind speed. As a result of severe storm, some meteorological stations have new extreme values that the strongest wind speed measured was 81 knots in the central region of Turkey. Medicane with wind speed 81 knots especially over Turkey is a rare event. This devastating cyclone carried exceptionally very strong winds (>80 kts) with favorable conditions to follow windstorm conceptual model. The cyclone caused adverse conditions such as excessive injuries, fatal incidents and forest fires. Mesoscale vortex formed and affected particularly the middle and western regions of Turkey. The vertical thermodynamic structure of storm is compared with April values of 40 years of datasets over Istanbul. Moreover, four different winds {measurement masts} of Istanbul Atatürk Airport are used for the microscale analysis of different meteorological parameters during deepened pressure level. In addition, divergence and vorticity of stormy weather are discussed in details during the effective time period of storm by solving equations and validated using ERA-40 reanalysis. We obtained many monitoring data sources such as ground base, radar, radiosonde and satellite display the values of the intensity of wind speed caused by cyclones of tropics have revealed similarities.

✉ Sevinc A. Sirdas
sirdas@itu.edu.tr; ssirdas@gmail.com

[1] Department of Meteorological Engineering, Faculty of Aeronautics and Astronautics, Istanbul Technical University, 34469 Maslak, Istanbul, Turkey

[2] Turkish State Meteorological Service, Atatürk Airport Meteorology Office, Yeşilköy, İstanbul 34149, Turkey

[3] Department of Earth, Ocean and Atmospheric Sciences, Florida State University, Tallahassee, FL 32306, USA

Keywords Tropical cyclone · Extreme weather · Severe storm · Mesoscale weather · African dust · Divergence—vorticity

1 Introduction

The cyclones that are controlling the weather and climate of the Mediterranean Basin are categorized according to their severity and occurrences. There are five groups of middle latitude cyclones that are entering from outside of the Mediterranean Basin of the thermal low-pressure, downwind cyclones, including wave cyclones and troughs. The majorities of cyclones of Mediterranean region develop into the form of "downwind/wave cyclones." In this form, depression rates are higher than all other categories around 69 or 91% annually. The cyclones occur in the western, eastern and central Mediterranean region and south of the Atlas Mountains (Türkeş 2010).

Windstorm conceptual model deals with the life cyclone of the cyclone based on the intensity of nature of jet (cold, warm and exceptionally strong winds). The present cyclone had most rapid deepening with strong winds (Hewson and Neu 2012). Examination of the storm occurrence region depended on the investigation of source areas. The majority of the researches have been devoted to the track of the cyclone from monthly, seasonal and even yearly data. Deniz et al. (2012) examined the source region of systems that affected the Marmara region, Turkey, between 2000 and 2010. They found that 31.54% of the storms occurred as a result of the low pressure of the central Mediterranean systems. Additionally, the explorations of extreme weather events that have occurred in Turkey and over the other source regions (Mediterranean is excluded) are also affecting the weather of Turkey. There are a number of studies about paths and extremes of storms in Turkey e.g., (Alpert et al. 1990a, b; Deniz and Karaca 1995; Deniz et al. 1997; Karaca et al. 2000; Tayanç et al. 1998; Kömüşçü et al. 2011; Toros et al. 2010; Türkeş 1996, 1998, 2004; Turoğlu 2010; Koç et al. 2005a, b; Sirdas 2005 and Sirdas et al. 2007; Şahin 2002).

Unger (1996) in his study presented that when Mediterranean storms are observed in the west of Hungry, the heat island intensity (the difference of temperatures between a central urban site and a rural site) is too low, approximately 0.68 °C; it has been explained by the presence strong snow and rain along with warm front of Mediterranean cyclone. If Hungary is found in the east of Mediterranean cyclone, the very low heat island approximately 0.83 °C; this could be explained the severity of cold front caused by stormy winds.

Bartzokas et al. (2002) in their study found November and December as the windy months from the analysis of annual wind in Ioannina region (in Greece), and furthermore, they found that it is due to the effect of Mediterranean cyclone. Flocas et al. (2009) studied the orbits of cyclone developed over Mediterranean Sea. They showed the beginning of low-pressure areas which develop significantly on the Balkan Peninsula in April. Mascatello et al. (2008) simulated the cyclone of September 26, 2006, with WRF (Weather and Research Forecasting) in southeastern Italy. The reason for this is that the lowest ever pressure is measured as 984 hPa on the same day. According to their experiment, the cyclone development started with a low-pressure system formation and the cyclonic system travelled through over the Mediterranean Sea, to pass the Ioannina Sea, and finally reached the Salento Peninsula across the Adriatic Sea and further reached the northern part of the Aquila.

Sirdas (2005) studied the harmonic analyses of daily wind data for 10 meteorological stations in Marmara region. The stations of Gökçeada, Bozcaada and Çanakkale have had higher wind speed values since their harmonic numbers have greater variations. In a similar study, Deniz et al. (2012) examined the storms of Marmara region between 2000 and 2010. These studies explored the cause of the storms due to low-pressure systems in central Mediterranean Basin affecting parts within the Marmara region. Hruska (2006) investigated the effects of a wind storm in the western side of the Wasatch Range on April 23, 1999. Wind speed rated up to 165 knots from the city airport to Brigham and caused serious damages to the city and the surrounding of Wasatch area. He mentioned in his paper that the two main elements created the down slope windstorms, which were the mountain waves produced from the upslope flow and the gap flow.

Stuart and Grumm (2006) also studied a new method to provide information about strong storms for forecasters by using the long-term normalized data. However, the main purpose of the article is to examine the wind anomalies over the east coast of America. Saaroni et al. (1997) checked the storms in eastern Israel. They analyzed the frequencies of the easterly storms and origin of their synoptic systems.

Zhao et al. (2008) considered the observation between 2000 and 2006 in order to show that Asian dust storm moved along Pacific to North America (Zhao et al. 2008). Therefore, the values of particulate matter (PM) or particulates had high correlation approximately 83% associated with dust storms in this region. The measurements between 2000 and 2006 showed three factors that caused higher relation between dust storms and PM values. They are: (a) the force of extend cyclones along Mongolia to northeast China: The frontal cyclones not only bring cold weather, but they also source the dust storm in East Asia and flow around the dust particles in the Pacific. In addition, they carry dust storm vertically to reach upper prevailing western wind in the troposphere. (b) The trans-Pacific transport route is controlled by the circulation tracks of westerlies over the NorthPacific. Western jets of strong zonal flow affect the Asiatic dust which travels to North Pacific via the path of Trans-Pacific. (c) Precipitation is one of the most important factors in reducing the transportation of Asiatic dust.

Grumm and Lambert (2010) studied maximum wind speed of 40–50 knots of the western wind zone as a result of a frontal development in Pennsylvania on April 16, 2010. These events have reported severe damage due to impacts of the wind. According to the study of Cavicchia et al. (2014), the number of cyclone (medicane) of 1.6 per year over whole Mediterranean region is rare.

Grumm (2010) examined another strong storm effective Western Europe States on February 27–28, 2010. The storm entered through the grounds of west Portugal. It increased the severity of the storm on land and caused heavy rains. There were 62 fatal cases reported due to the calamity: 51 in France and 11 in the rest of Europe. This article examined the circumstances that created the storm by using different levels of data such as the geopotential height at 500 mb, the temperature at 850 mb and wind speed at 850 mb. Goyette (2011) examined the wind speeds of storms and their synoptic conditions, which occurred in Switzerland. The objective of this study includes the following: (i) investigation of the surface conditions of the stormy winds, (ii) directions and magnitude of the strongest wind at Turkey region, from which the storms passed, (iii) linking strongest wind with other systems and (iv) whether there was any relationship between the ocean currents, dust storms and stormy winds.

2 Brief synoptic history of Mediterranean cyclone

Energy and moisture from Mediterranean Sea generate the cyclones and unique weather features of Mediterranean region. Mesoscale location of this region is lying between mid-latitude westerlies and the subtropical high-pressure belt. General character of Mediterranean is being a generator of cyclones or influenced by neighboring weather system as a closed-basin system (Lionello and CMCC 2012; Trigo et al. 1999, 2000). Lionello et al. (2006) and Buzzi and Tibaldi (1978) described the generation of Mediterranean cyclone as the orographic cyclogenesis due to structure of the region. The intensity and duration of Mediterranean cyclones have distinct character than that of Atlantic Ocean or Pacific Ocean such as shorter lifetime, heavy rain and strong winds. In this study, the cyclone is generated on the Sahara Desert (northern Africa) since the warming of area generates strong temperature difference between Mediterranean Sea (Alpert and Ziv 1989). The local variability shows complex features that linked precipitation and wind, e.g., strong winter cyclone activity over Italian peninsula and strong summer cyclone on Iberian and North Africa (Trigo et al. 1999). There is seasonal change in cyclogeneses found in winter, spring and summer. Winter cyclones are intense and distributed over larger area (middle and east coast Mediterranean), and spring cyclone is dominant over North Africa, known as Saharan cyclones (Lionello et al. 2006; Trigo et al. 1999). The lee of Alps cyclogenesis is connected with Saharan lows residing on radiative heating from desert dust (Buzzi and Tibaldi 1978; Egger et al. 1995; Thorncroft and Flocas 1997).

The cyclone originated in North Africa caused strong storms in western and middle of Turkey on April 18, 2012. The dust particles from North Africa carried with the strong wind caused the drop in pressure. Dust particles contained in the dust storm reduced the visibility around 1 km in many places. As a consequence of the storm, the new values were historically high, over some of the meteorological stations. The values of a fresh extreme cyclone were the highest values, recorded at the district of Elmadağ Province of Ankara around 81 knots. Other extreme values were measured at Datça, 74 knots; Cihanbeyli, 65 knots; Haymana, 61 knots; and Bala, 60 knots. On the same day, the other highest measured values were in Kumbet Automated Weather Observing System (AWOS) 77 knots and Amasra 68 knots.

This work is based on the wind speed more than 50 knots (described in detail in Sect. 4). Figure 1 displays the maximum wind speed values which exceeded 50 knots during the 6-h interval. The stormy day was effective at southwestern regions of Turkey and begins to strengthen depending upon the influence of the low-pressure and frontal systems at April 18, 2012, 0000 UTC and 0600 UTC (Fig. 1a, b). Storm had begun to spread from wider areas from 0800 UTC. The cold front was dependent on the occlusion front systems centered over northern Aegean regions between 1000 UTC and 1030 UTC. The winds became stronger while it was passing through northwestern part of Turkey. Storm after being effective on large areas continued to be observed over several stations until 1530 UTC (Fig. 1c). The center of pressure developed in the area of Giresun and Gümüşhane around 988 hPa on 1800 UTC. The center became stronger due to highest pressure gradient and the factor of height over east and north of Turkey after this time, as shown in Fig. 1d. The maximum values were measured at the AWOS of Kümbet (1730 m height) and the Ski Center of Zigana (2050 m height) as 77 knots and 53 knots maximum values, respectively, after 1800 UTC.

The low pressure centered a wide region area as a part of 1004 hPa isobar over Libya and the Lake of Chad Lake, and it deepened to 1000 hPa in the southern Libya, Nigeria and

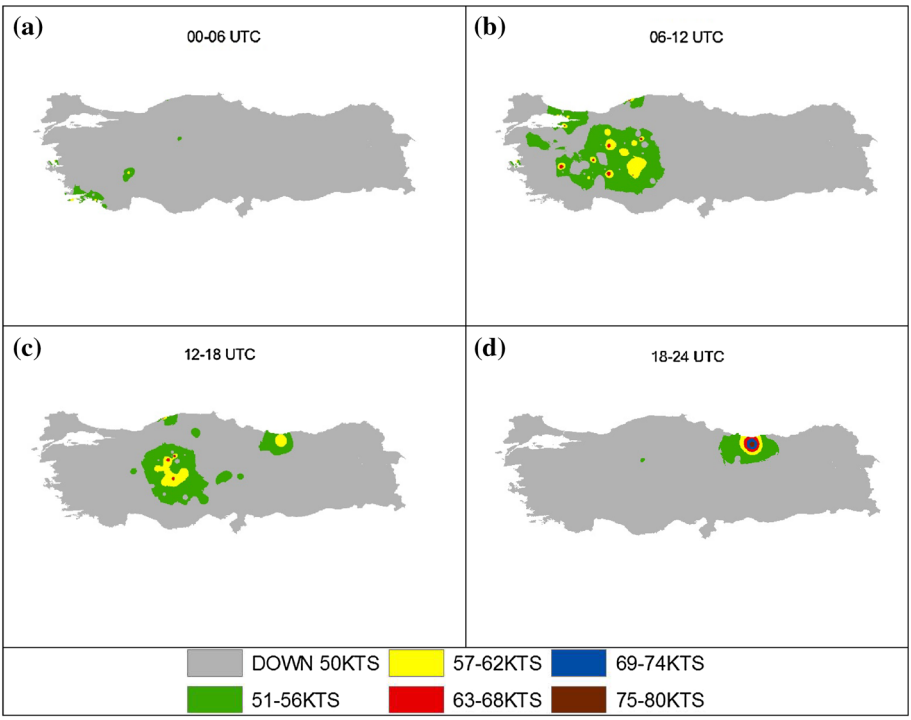

Fig. 1 Representation of the maximum wind speed exceeds, 51 knots each stations in 6-h interval, given in the map of Turkey on April 18, 2012; **a** from 0000 UTC to 0600 UTC, **b** from 0600 UTC to 1200 UTC, **c** from 1200 UTC to 1800 UTC, **d** from 1800 UTC to 2400 UTC

Chad Republic (Fig. 2a–d). The center of low pressure moved to the north and northeast on 17 April 1800 UTC, and then, it reached 996 hPa values over the southwest of Crete Island, northeast of Libya and northwest of Egypt (Fig. 2d–h). The center maintained its strength around 996 hPa on 18 April 0000 UTC (Fig. 3a); the southeast part of Turkey began to receive wind stronger than 50 knots due to the influence of the low-pressure system. At 0600 UTC, the cyclone center acquired the lowest value 988 hPa (Fig. 4a); at 1200 UTC, it started to fill up with 992 hPa value by expanding through Turkey's Marmara region (Fig. 5a). It progressed to north and northeast at 1800 UTC by maintaining its value around 992 hPa; however, it began to reduce the impact on Turkey.

3 Study area and data

The evaluation of surface winds data for entire Turkey is acquired by using the meteorological observations and measurements that belong to AWOS of Turkish State Meteorological Service (MGM). Saaroni et al. (1997) described three necessary conditions to define a storm. One of them has been used in this study and is defined as "winds greater than 50 knots" by Deniz et al. (2012). Ground base wind data that belonged to April 18, 2012, were used to evaluate windy conditions and acquired from all Automated Weather Observing Systems (AWOS) and Airports of Turkish State Meteorological Services. The airports and AWOS wind speed data of storm are examined on the basis of the values

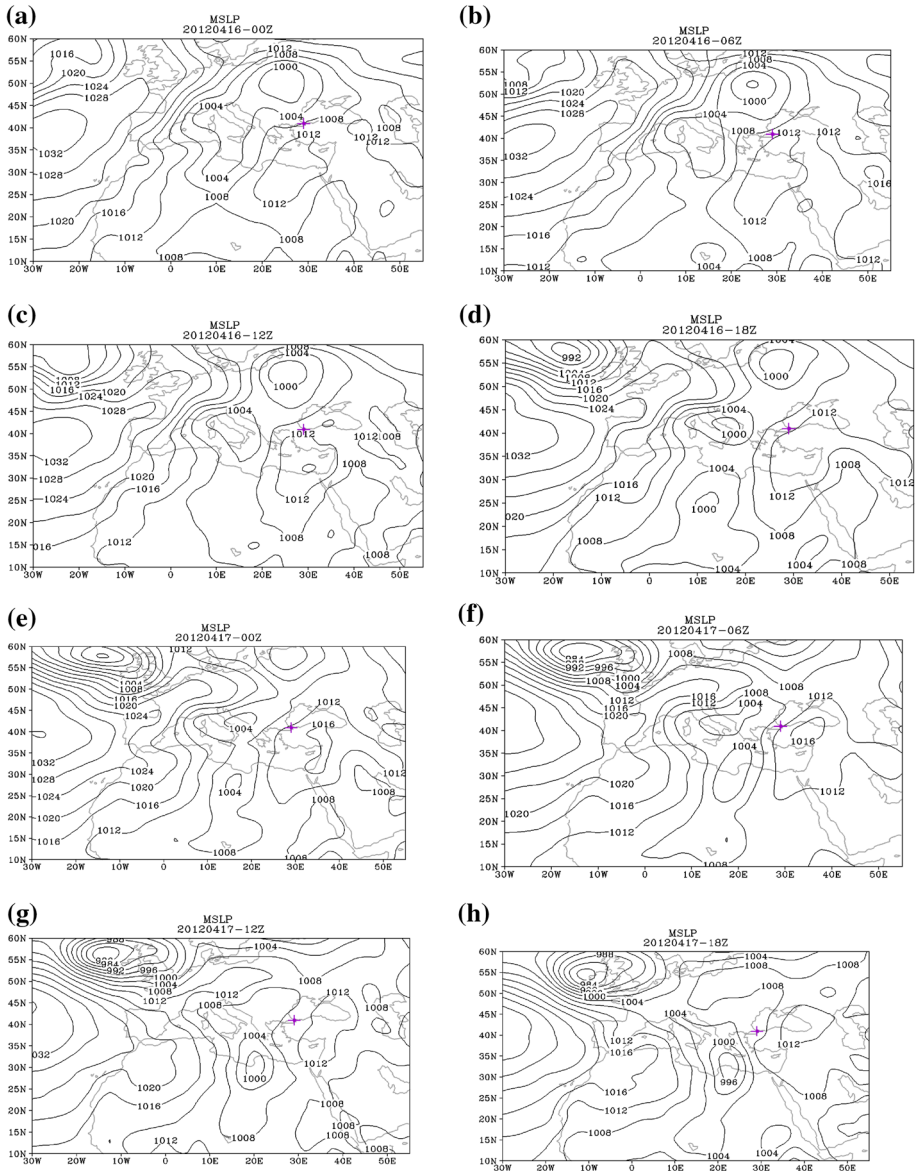

Fig. 2 Mean sea level pressure (hPa, *black lines*) maps produced by using NCEP/NCAR reanalysis data on April 16, 2012; **a** 0000 UTC, **b** 0600 UTC, **c** 1200 UTC, **d** 1800 UTC and also on April 17, 2012; **e** 0000 UTC, **f** 0600 UTC, **g** 1200 UTC, **h** 1800 UTC

greater than 50 knots in this study. The new extreme values of some meteorological stations were measured as a result of the storm on April 18, 2012. A new excessive value of cyclone was recorded as 81 knots during passage of this storm in Elmadag District of Ankara Province. The extreme values on that day were 74 knots in Datca, 65 knots in Cihanbeyli, 60 knots in Haymana and 60 knots in Bala. The other highest measured values were 77 knots in AWOS of Kumbet and 68 knots in Amasra.

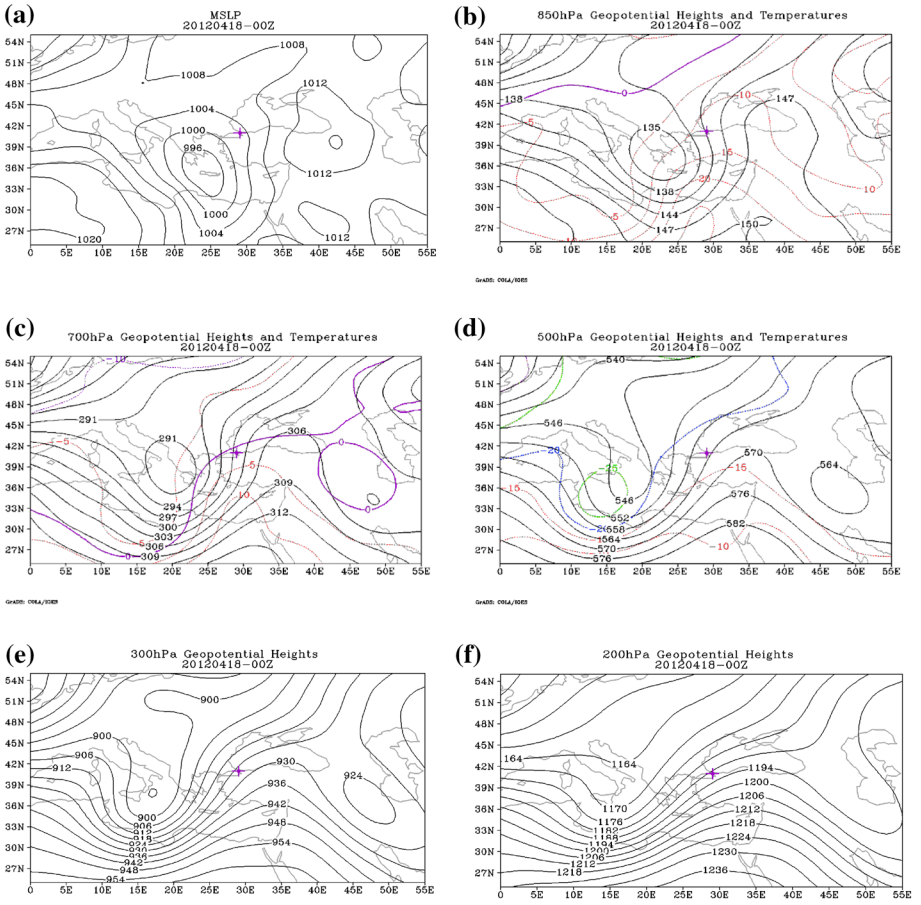

Fig. 3 Maps of geopotential heights (m/10, *black lines*) and temperatures (in Celsius, colorful and drawn 5 °C intervals) produced by using NCEP/NCAR reanalysis data on April 18, 2012, 0000 UTC; **a** the average sea level pressure (hPa, *black lines*), **b** 850 hPa, **c** 700 hPa, **d** 500 hPa, **e** 300 hPa, and **f** 200 hPa

In this study, the examination of the NCEP/NCAR reanalysis of 2 data products (Kalnay et al. 1996) is applied on two separated domains, including one big domain and one small domain. Bigger area was placed between 30 W–55E and 10 N–60 N, and small domain was positioned between 00E–55E and 25 N–55 N. Time period of evaluation was selected from April 10, 2012, 0000 UTC to April 22, 2012, 1800 UTC, and products recorded 6-h intervals by plotting meteorological maps.

Skew-T (sounding) diagrams were used from the Web site which belongs to the University of Wyoming. The skew-T/log-P diagrams of April 18, 2012, 1200 UTC in İstanbul were compared with the diagrams of the values of the month of April between 1970 and 2011. This comparison shows how much deviation was measured from the average values in Tables 1 and 2.

For microscale study of meteorological parameters in Istanbul Atatürk Airport (IST/AHL), wind masts data were acquired from 4 different locations, during the storm pass. The divergence and vorticity of the most effective time period variations are discussed in details for the IST/AHL Airport.

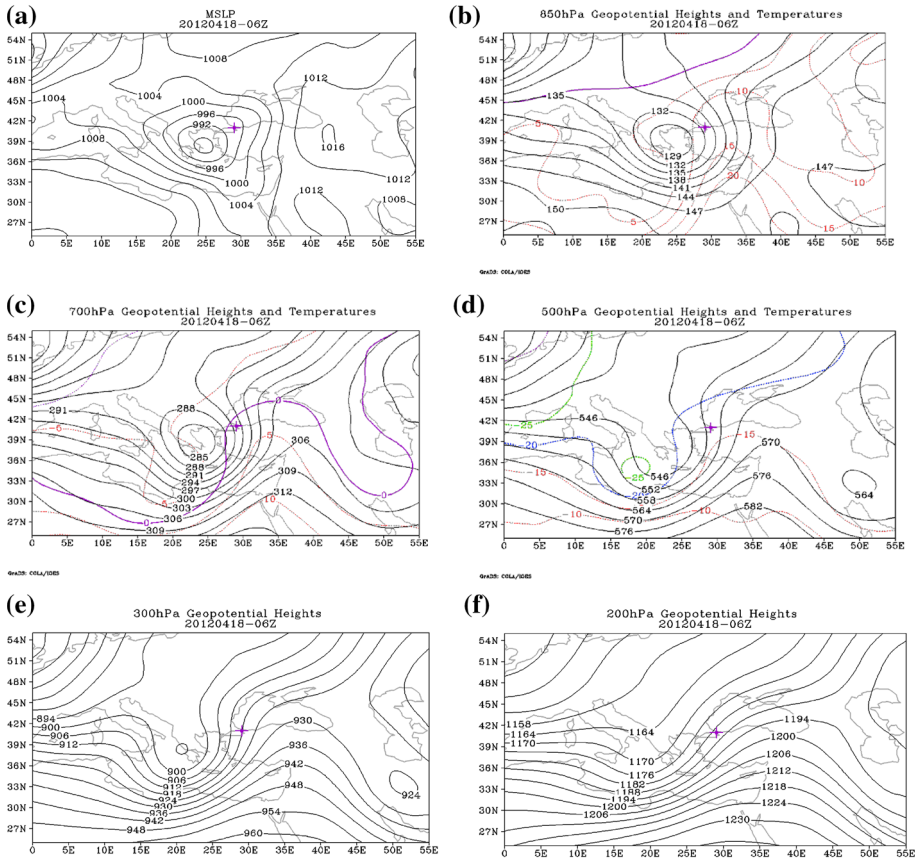

Fig. 4 Maps of geopotential heights (m/10, *black lines*) and temperatures (in Celsius, colorful and drawn 5 °C intervals) produced by using NCEP/NCAR reanalysis data on April 18, 2012, 0600 UTC; **a** the average sea level pressure (hPa, *black lines*), **b** 850 hPa, **c** 700 hPa, **d** 500 hPa, **e** 300 hPa and **f** 200 hPa

4 Initial genesis sequence

4.1 Sea and upper-level pressure maps

The low-pressure center established over Sicily, Sardinia and Italy as value of 992 hPa on April 13, 2012. The maps of 500 hPa show the contours of 552 dam extending from Balkans to Sahara and Portugal. There was a 992 hPa low-pressure center over Adriatic Sea on April 14, 2012. The upper-level 500 hPa 552 dam contours expanded from western part of Turkey to northern parts of Africa and Portugal. On 15 April, two low-pressure centers occurred over Romania as 996 hPa, and another over Libya and Egypt as 1012 hPa. The upper-level 500 hPa contour of 552 dam moved from the west of Turkey to the south of Sahara and Portugal. In addition, the brief synoptic history of cases is given in Table 3 which summarized the synoptic conditions from the initial genesis that began on April 13, 2012, to the cyclone left on April 18, 2012, over Turkey according to the mean sea level pressures, the geopotential heights and the wind speeds.

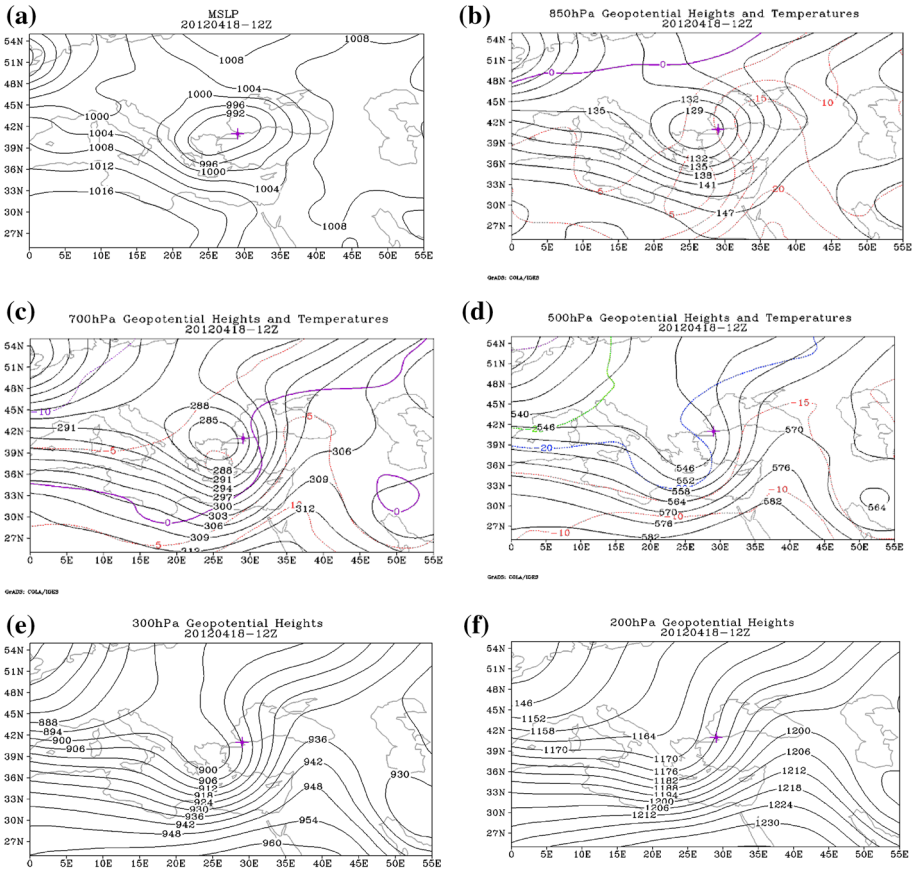

Fig. 5 Maps of geopotential heights (m/10, *black lines*) and temperatures (in Celsius, colorful and drawn 5 °C intervals) produced by using NCEP/NCAR reanalysis data on April 18, 2012, 1200 UTC; **a** the average sea level pressure (hPa, *black lines*), **b** 850 hPa, **c** 700 hPa, **d** 500 hPa, **e** 300 hPa and **f** 200 hPa

4.1.1 The synoptic situation of mean sea level pressure on April 16, 2012

The trough of low pressure centered at upper level of Eastern Europe; its value became 1000 hPa in Italy and 1008 hPa in Libya at 0000 UTC. There was a low-pressure center over great Sahara Desert around 1008 hPa and a high-pressure center over Atlantic Ocean about 1032 hPa (Fig. 2a). After 6 h at 0600 UT, 1000 hPa low-pressure center in Eastern Europe deepened to reach 996 hPa; moreover, a part of the low-pressure center broke off to move over Italy, Malta, Sicily and Sardinia with 1004 hPa value. Pressure 1008 hPa isobar merged into another 1008 hPa isobar above great Sahara Desert to form 1004 hPa low-pressure center of Lake Chad (Fig. 2b). A low-pressure center of 1000 hPa formed in Eastern Europe, and another low-pressure center occurred in Italy and Sicily as 1004 hPa value at 1200 UTC (Fig. 2c). The pressure at 1800 UTC remained same in Eastern Europe at 1000 hPa, Italy and Sicily 1004 hPa. After 1800 UTC, 1004 hPa pressure center above Italy deepened over Adriatic Sea by decreasing pressure to 1000 hPa. The great Sahara Desert has reached the value of 1000 hPa, and the low-pressure center extended as the upper-level trough of 1004 hPa from Libya to the central Mediterranean region (Fig. 2d).

Table 1 Comparison of upper air soundings for April's average from 1970 to 2011 and April 18, 2012, 1200 UTC

Pressure levels (hPa)	Variables	Average of April from 1970 to 2011	18 April 1200 UTC	Pressure levels (hPa)	Average of April from 1970 to 2011	18 April 1200 UTC
850	Mean height (m)	1464.2	1285	100	16,157.8	16,270
	Minimum height (m)	1307	1285		15,787	16,270
	Mean temperature (°C)	5.2	8.2		−57.5	−55.5
	Mean wind speed (knots)	29.7	46		52.9	13
	Mean humidity (%)	59.6	61		5.2	1
700	Mean height (m)	3020.9	2863	50	20,510.5	20,580
	Minimum height (m)	2667	2863		19,689	20,580
	Mean temperature (°C)	−4.3	0		−58.4	−58.5
	Mean wind speed (knots)	36.9	27		34.8	11
	Mean humidity (%)	54.9	55		4.5	1
500	Mean height (m)	5588.4	5450	30	23,737.6	23,800
	Minimum height (m)	5319	5450		–	23,800
	Mean temperature (°C)	−21.4	−18.9		−55.9	−57.7
	Mean wind speed (knots)	–	64		33.2	11
	Mean humidity (%)	42	68		4.1	1
300	Mean height (m)	9146.5	9060	20	26,335.3	26,380
	Minimum height (m)	8761	9060		24,503	26,380
	Mean temperature (°C)	−48.4	−40.9		−52.6	−54.9
	Mean wind speed (knots)	77.2	64		39.9	14
	Mean humidity (%)	31.5	9		3.5	1

Table 1 continued

Pressure levels (hPa)	Variables	Average of April from 1970 to 2011	18 April 1200 UTC	Pressure levels (hPa)	Average of April from 1970 to 2011	18 April 1200 UTC
200	Mean height (m)	11,748.4	11,760	10	30,905.9	30,920
	Minimum height (m)	10,334	11,760		28,264	30,920
	Mean temperature (°C)	−56.2	−48.1		−43.5	−45.5
	Mean wind speed (Knots)	74.3	46		66.7	26
	Mean humidity (%)	15.3	3		2.5	1

Table 2 Anomalies computed for April 18, 2012, 1200 UTC and April's average from 1970 to 2011

Pressure levels (hPa)	Mean height (m)	Minimum height (m)	Mean temperature (°C)	Mean wind speed (knots)	Mean humidity (%)
850	−179.2	−22	3	16.3	1.4
700	−157.9	196	4.3	−9.9	0.1
500	−138.4	131	2.5	–	26
300	−86.5	299	7.5	−13.2	−22.5
200	11.6	1426	8.1	−28.3	−12.3
100	112.2	483	2	−39.9	−4.2
50	69.5	891	−0.1	−23.8	−3.5
30	62.4	–	−1.8	−22.2	−3.1
20	44.7	1877	−2.3	−25.9	−2.5
10	14.1	2656	−2	−40.7	−1.5

4.1.2 The synoptic situation of mean sea level pressure on April 17, 2012

A 1036 hPa of the high-pressure center formed on 0000 UTC above the Atlantic Ocean. This is connected to an upper-level ridge above central Europe and also continuing to Algeria and Sahara with 1020 hPa pressure. The low-pressure center on the Adriatic Sea and Libya is 1004 hPa, and the high-pressure center is expanded on the center of Turkey and Israel with 1016 hPa value (Fig. 2e, f). The 1004 hPa low-pressure center located in Libya lengthened its area through Libya and central Mediterranean region. The map of 500 hPa is shown in Fig. 3d, the low-pressure center of 546 dam above Corsica and Sardinia. The low-pressure center deepens above Libya and central Mediterranean at 1200 UTC, and the low-pressure center of 1000 hPa is formed over the southern of central Mediterranean Sea and Libya. The 1016 hPa high-pressure center has lost its strength up to

Table 3 Brief synoptic history of various cases

Case date	Mean sea level pressure	Upper-level pressure	Winds at 10 m
April 13, 2012	Low-pressure center established over Sicily, Sardinia and Italy as value of 992 hPa	The contours of 552 dam extended from Balkans to Sahara and Portugal at 500 hPa	–
April 14, 2012	There was a 992 hPa low-pressure center over Adriatic Sea	The 552 dam expanded from west of Turkey to North Africa and Portugal at 500 hPa	–
April 15, 2012	Two low-pressure centers occurred over Romania, Libya and Egypt. Pressure varied from 996 to 1012 hPa	The 552 dam moved from the west of Turkey to the south of Sahara and Portugal at 500 hPa	–
April 16, 2012	Low-pressure center over Eastern Europe divided two above Italy and Libya. It divided three over Sahara Desert, Italy and East Europe. Pressure varied from 996 to 1008 hPa	The trough of low pressure centered over Eastern Europe extended from Sahara Desert, Lake Chad to the central Mediterranean region at 500 hPa	–
April 17, 2012	Low-pressure center located in Libya lengthened its area through Central Mediterranean. It deepened and moved over the southwest of Crete and north of Libya. Pressure varied from 996 to 1004 hPa	Atlantic Ocean high-pressure center of 1036 hPa connected to an upper-level ridge above central Europe, Algeria and Sahara. 546 dam over of low-pressure center formed on Corsica and Sardinia. The 552 dam moved North Africa at 500 hPa	–
April 18, 2012, 0000 UTC	The low center is situated at the Crete Island with 996 hPa value. The cold front beginning from the north of Crete passed to Egypt through Libya while the warm front starting from the same place moved to Greece, Bulgaria and Romania	The low pressure of 135 dam is located in the Peloponnese Peninsula of Greece at 850 hPa. The trough is extended from the southeastern of Italy to the north of Africa	The southerly flow starting from Libya and Egypt travelled through the west and south of Turkey. westerly winds varied from 40 knots to 140 knots
April 18, 2012, 0600 UTC	A deepening low center moved to the North Aegean Sea, Greece and North Africa. The cold front starting from the North Aegean Sea passed through the southwest of Turkey to Egypt. The warm front beginning from the same place moved to Greece, Bulgaria and the northwest of Black Sea. The isotherm of 0 °C spread to the west of Turkey. Pressure varied from 896 to 988 hPa	Low pressure of 129 dam and 285 dam were located on the Central Aegean Sea at 850 hPa and 700 hPa. The 546 dam is moved from Russia to west of Turkey extending through North Africa at 500 hPa and 300 hPa. Moreover, the trough at 200 hPa deepened and spread from Adriatic Sea to North Africa	Westerly, southerly and southeasterly winds reached 30 knots, 45 knots, 50 knots and 60 knots from surface to 700 hPa. The horizontal jet core speed was 130 knots with vertical speed 80 knots at 500 hPa and 100 hPa

Table 3 continued

Case date	Mean sea level pressure	Upper-level pressure	Winds at 10 m
April 18, 2012, 1200 UTC	Deepened low-pressure center is moved to the northeast. It placed Marmara region with the value of 992 hPa. The occlusion front started over the North Aegean, and it moved from Bulgaria to Black Sea. The warm front began on the west Black Sea and Russia; the cold front occurred on the west Black Sea, Cyprus and Egypt. The isotherm of 0 °C is stretched from the east of Marmara toward the east of Antalya. The contour of −20 °C is located over North Africa, Italy and Turkey	The low pressure of 129 dam stated the west Aegean Sea, Marmara Region, Bulgaria and Greece at 850 hPa. 285 dam is located in the north of Aegean Sea, Greece and the northwest of Turkey at 700 hPa. 546 dams move from Russia to Italy, Crete and Istanbul At 500 hPa. The trough of 900 dams passes from Turkey and Greece to northern Africa. Map of 200 hPa displays the trough located in the south of Italy and North Africa	The center and western part of Turkey was influenced by south and southeastern wind flows by cyclonic rotation. Winds varying from westerly 35 knots to 120 knots from Egypt to Turkey

Turkey (Fig. 2g). As shown in Fig. 2h, the low-pressure center of 996 hPa became stronger over the southwestern part of Crete and north of Libya at 1800 UTC. The 1012 hPa high-pressure center is located above the northeast of Turkey and the Caucasus (Fig. 2h). The contour of 552 dam moved to North Africa as seen from the map of 500 hPa.

4.1.3 The synoptic situation of mean sea level pressure on April 18, 2012, 0000 UTC

On 18 April 0000 UTC, the pressure center is situated at the Crete Island in the Mediterranean Sea with 996 hPa value. The southerly flow starting from Libya and Egypt travelled through the western and southern part of Turkey (Fig. 3a). The cold front beginning from the north of island Crete passed to Egypt through Libya, while the warm front starting from the same place moved to Greece through Bulgaria and Romania. Low center of 850 hPa of 135 dam is located in the Peloponnese Peninsula of Greece (Fig. 3b). The trough is extended from the southeast of Italy to the north of Africa (Fig. 3c–f).

4.1.4 The synoptic situation of mean sea level pressure on April 18, 2012, 0600 UTC

On April 18, 2012, 0600 UTC, a deepening low-pressure center moved to north of the Aegean Sea, and it reached the value 988 hPa (Fig. 4a). The west and south of Turkey interior regions stayed fully under constant wind flows. The pressure gradient over Turkey is approximately 8.5 hPa/250 km. The cold front starting from the northern Aegean passed through the southwest of Turkey to Egypt, and the warm front beginning from the same place moved through Greece, Bulgaria and to the northwest of Black Sea. The low center of 129 dam is located on the Central Aegean Sea as shown in the map of 850 hPa (Fig. 4b). The contour of low pressure with 285 dam is set on the Aegean Sea and Greece from the map of 700 hPa; furthermore, zero degrees' isotherm spread from northwest to southwest of Turkey (Fig. 4c). The contour of 546 dam moved from Russia to west of Turkey extending through North Africa as seen in the map of 500 hPa. The cold isotherm of

−25 °C is located above the central Mediterranean Sea (Fig. 4d). The low center occurred over Aegean Sea and Greece at 300 hPa, and it spread out to North Africa (Fig. 4e). Moreover, as given, the map of 200 hPa (Fig. 4f) deepened trough spread from Adriatic Sea to North Africa.

4.1.5 The synoptic situation of mean sea level pressure on April 18, 2012, 1200 UTC

The low-pressure center is moved to the northeast on April 18, 2012, at 1200 UTC. It spreads to the wider area including the north of Aegean Sea and whole of Marmara Region with the value of 992 hPa (Fig. 5a). The center and western parts of Turkey are influenced by south and southeastern wind flows. The pressure gradient on Turkey is approximately 3.4 hPa/250 km. The occlusion front started over the North Aegean, and it moved from Bulgaria to the Western Black Sea. While the warm front began on the west Black Sea and goes to Russia, the cold front occurred on the west Black Sea through Cyprus and Egypt. There is a low center of 129 dam stated the West Aegean Sea, Marmara region, Bulgaria and the East of Greece (shown from the map of 850 hPa; Fig. 5b). As given by the map of 700 hPa, the low center of 285 dam is located in the north of Aegean Sea, the east of Greece and the northwest of Turkey. The isotherm of 0 °C is stretched from the east of Marmara region toward the east of the Gulf of Antalya (Fig. 5c). The map of 500 hPa for 546 dams moves from Russia to Italy, Crete and Istanbul. The contour of −20 °C is located over North Africa, Italy and Turkey (Fig. 5d). The trough of 900 dams passes from Turkey and Greece to northern Africa (Fig. 5e). The map of 200 hPa displays the trough located in the south of Italy and north of Africa (see Fig. 5f).

4.2 Wind maps

4.2.1 The situation on April 18, 2012, 0000 UTC

The westerly 40 knots wind at 10 m is passing through the island of Crete, Egypt and Libya. It is extending from the northeast of Egypt to the west of Turkey, reaching 35 knots over Cyprus (Fig. 6a). Wind speed increased southwesterly 30 knots and 40 knots stretching from the southwest of Turkey at 1000 and 900 hPa (Fig. 6b, c). Southern winds at 700 and 850 hPa became 40 and 55 knots speed, respectively, which stretched from Libya to the west of Turkey (Fig. 6d, e). Jet's speed extended unusual values at distinct heights 90 knots, 120 knots, 140 knots, 110 knots and 75 knots, which moved from North Africa to western Turkey (Fig. 6f–l). There are two jets over the Mediterranean Sea, and their maximum core speeds are reaching 80 and 140 knots.

4.2.2 The situation on April 18, 2012, 0600 UTC

At 10 m, the western wind higher than 40 knots over Crete caused a cyclonic rotation due to which the south and southeastern winds are extended over the western part of Turkey (Fig. 7a). Westerly, southerly and southeasterly winds are reaching 30 knots, 45 knots, 50 knots and 60 knots at the altitude of 1000 hPa, 900 hPa, 850 hPa and 700 hPa, respectively (Fig. 7b–e). Six-hour interval between previous hours is compared with their jet core intensities at 500 hPa and 150 hPa levels. Jets have reduced the values around 10 knots at 400 hPa, 300 hPa and 250 hPa, and 20 knots at 200 hPa. Two jets located on the Mediterranean Sea have kept their position same. The horizontal jet core is 130 knots with

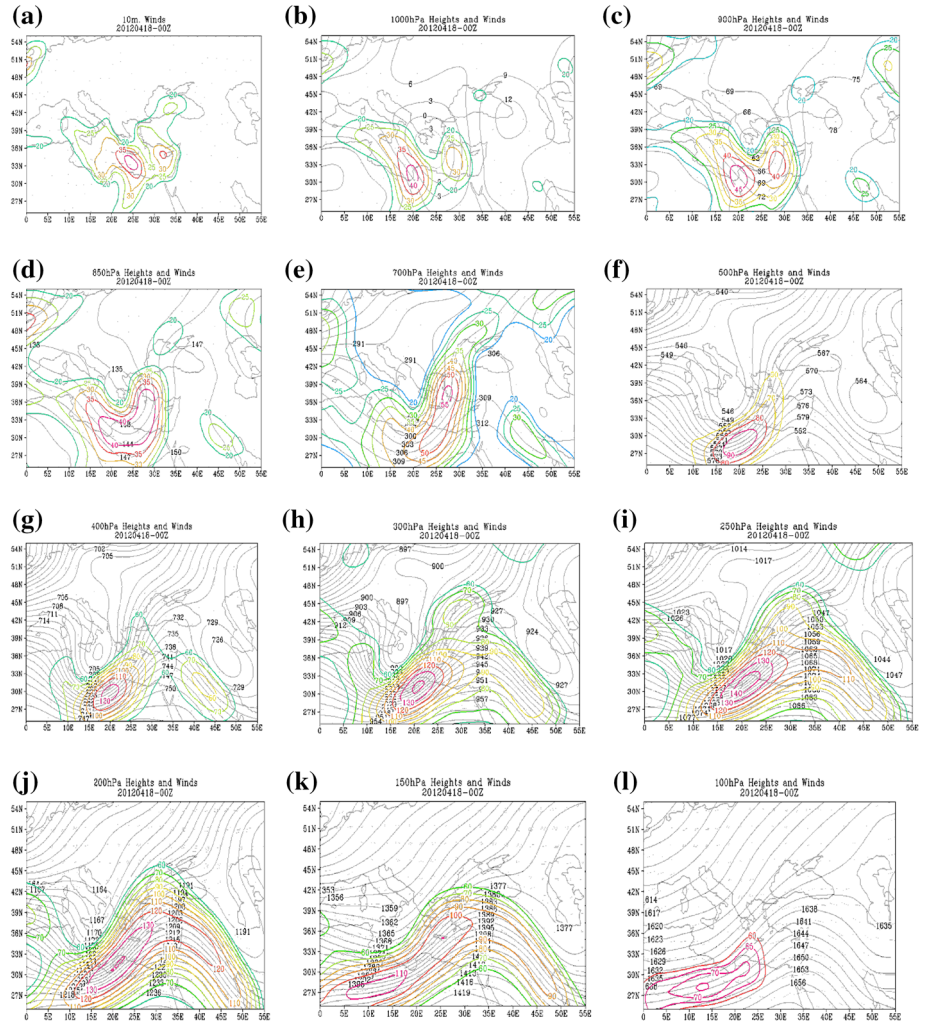

Fig. 6 Maps of geopotential heights (m/10, continuous *black lines*) and winds (isotachs; colored) produced by using NCEP/NCAR reanalysis data on April 18, 2012, 0000 UTC; **a** at 10-m winds, **b** 1000 hPa, **c** 900 hPa, **d** 850 hPa, **e** 700 hPa, **f** 500 hPa, **g** 400 hPa, **h** 300 hPa, **i** 250 hPa, **j** 200 hPa, **k** 150 hPa and **l** 100 hPa

vertical speed 80 knots altitudes between 500 hPa and 700 hPa. Wind speed of approximately 250 hPa level reaches horizontally 130 knots and vertically 80 knots on the top of level above 100 hPa (Fig. 7f–l).

4.2.3 The situation on April 18, 2012, 1200 UTC

Westerly winds of 35 knots at 10 m are located in the island of Crete located at 10 m; they caused the southern and southwestern winds extending toward western and central parts of Turkey by cyclonic rotation (Fig. 8a). At 1000 hPa, wind speed reached 35 knots between Crete and Libya, and the gusts reached out toward the inner parts and west of Turkey with

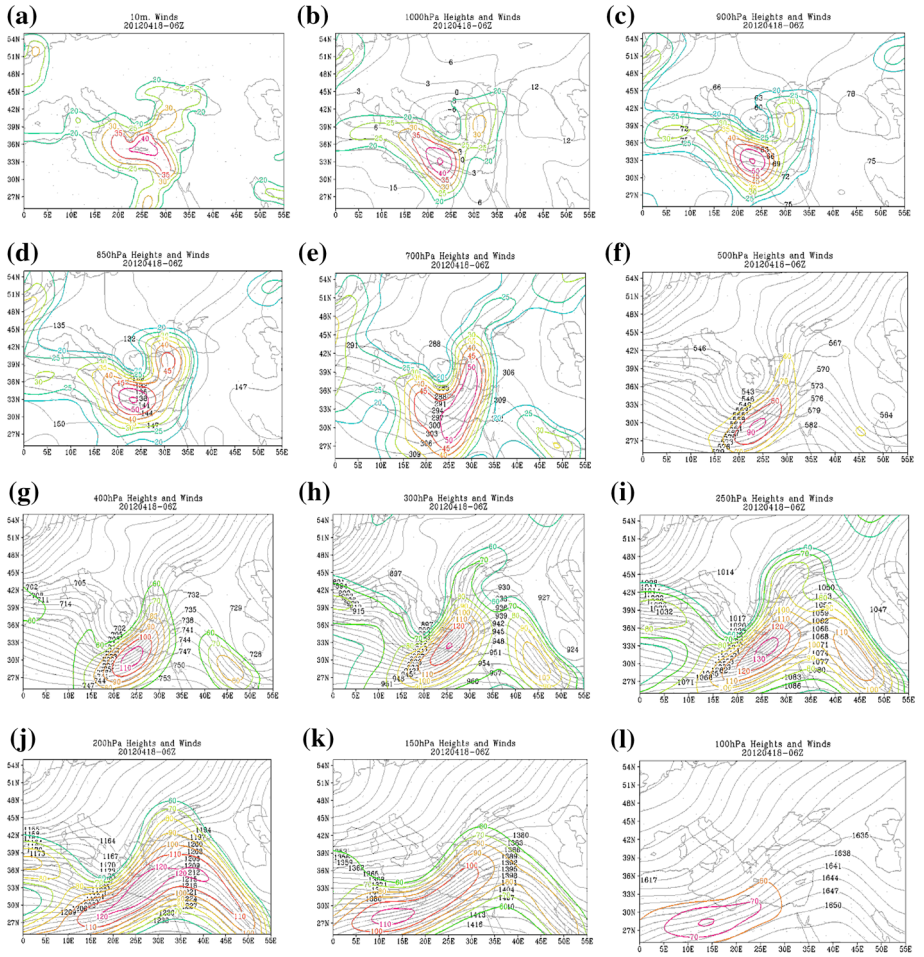

Fig. 7 Maps of geopotential heights (m/10, continuous *black lines*) and winds (isotachs; colored) produced by using NCEP/NCAR reanalysis data on April 18, 2012, 0600 UTC; **a** at 10-m winds, **b** 1000 hPa, **c** 900 hPa, **d** 850 hPa, **e** 700 hPa, **f** 500 hPa, **g** 400 hPa, **h** 300 hPa, **i** 250 hPa, **j** 200 hPa, **k** 150 hPa and **l** 100 hPa

25 knots speed (Fig. 8b). Maps of 900 hPa jets are reaching 40 knots among Libya and Crete so that the middle and western parts of Turkey are having the southerly wind around 35 knots (Fig. 8c). Wind speeds are increasing 40 knots and 55 knots at 850 hPa and 700 hPa (Fig. 8d, e). Jet core speeds are changing from 85 knots to 120 knots at different levels between 500 and 100 hPa (Fig. 8f–l). At 6 h compared to the previous jet values, they kept same values at 400 hPa, 200 hPa and 150 hPa but declined 10 knots and 5 knots between altitudes of 500 hPa and 100 hPa. Two jets have kept their position over Mediterranean region.

4.3 Satellite imagery

On April 18, 2012, 0000 UTC, the sand and dust from the deserts over northern part of Libya and Egypt moved on to the north of Crete Island and the south of Rhodes Island as

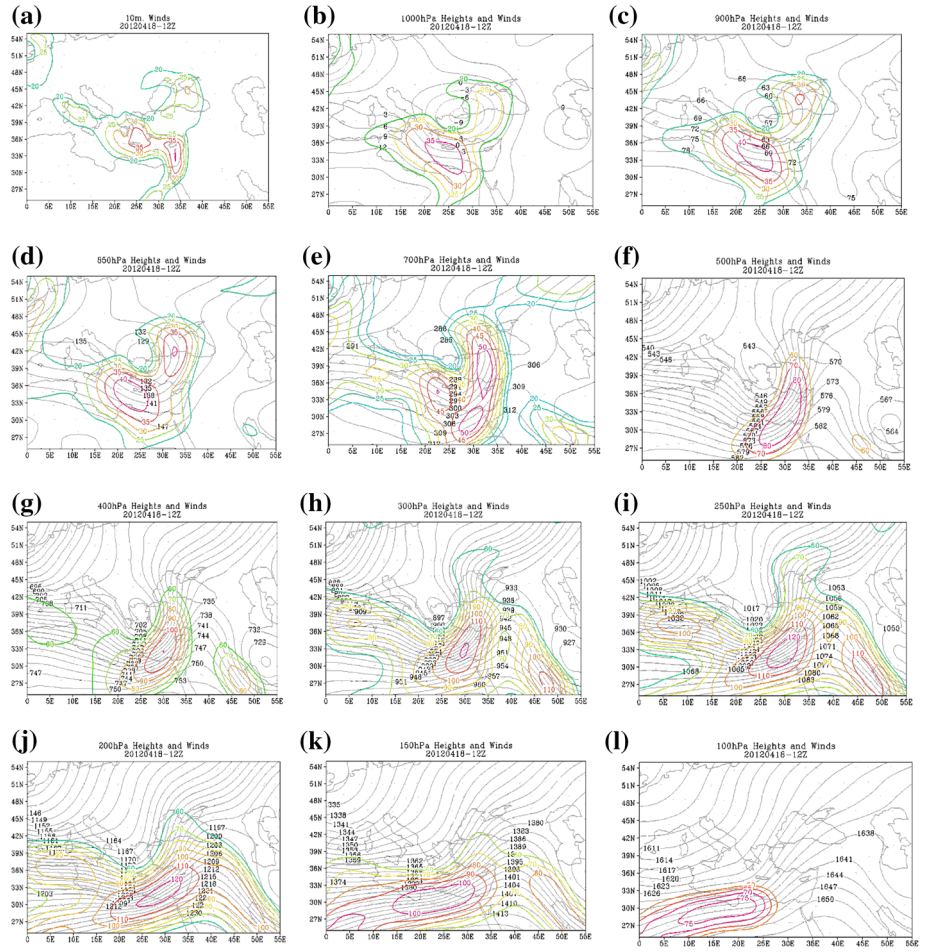

Fig. 8 Maps of geopotential heights (m/10, continuous *black lines*) and winds (isotachs; colored) produced by using NCEP/NCAR reanalysis data on April 18, 2012, 1200 UTC; **a** at 10-m winds, **b** 1000 hPa, **c** 900 hPa, **d** 850 hPa, **e** 700 hPa, **f** 500 hPa, **g** 400 hPa, **h** 300 hPa, **i** 250 hPa, **j** 200 hPa, **k** 150 hPa and **l** 100 hPa

shown in Fig. 9a–d. Satellite imagery taken in 15-min intervals shows that the dust can be seen moving toward the southwest parts of Turkey. Six hours later at 0600 UTC, the desert dusts from North Africa have started to impact the southwestern areas of Turkey on stormy day. Blowing dust is observed by the Meteorological Office of Bodrum Airport located in the southwest of Turkey at 0550 UTC (Fig. 9e–h). Dust can be seen from 15-min intervals in satellite images moving from the southwest of Turkey. At 1200 UTC, the effect of dust storms and their incidents are observed from the airports located in the northwestern and the central parts of Turkey. The visibility has decreased around 110 m at Konya Airport. The dust storm movement can be seen over central regions of Turkey by the satellite imagery in Fig. 9i–l.

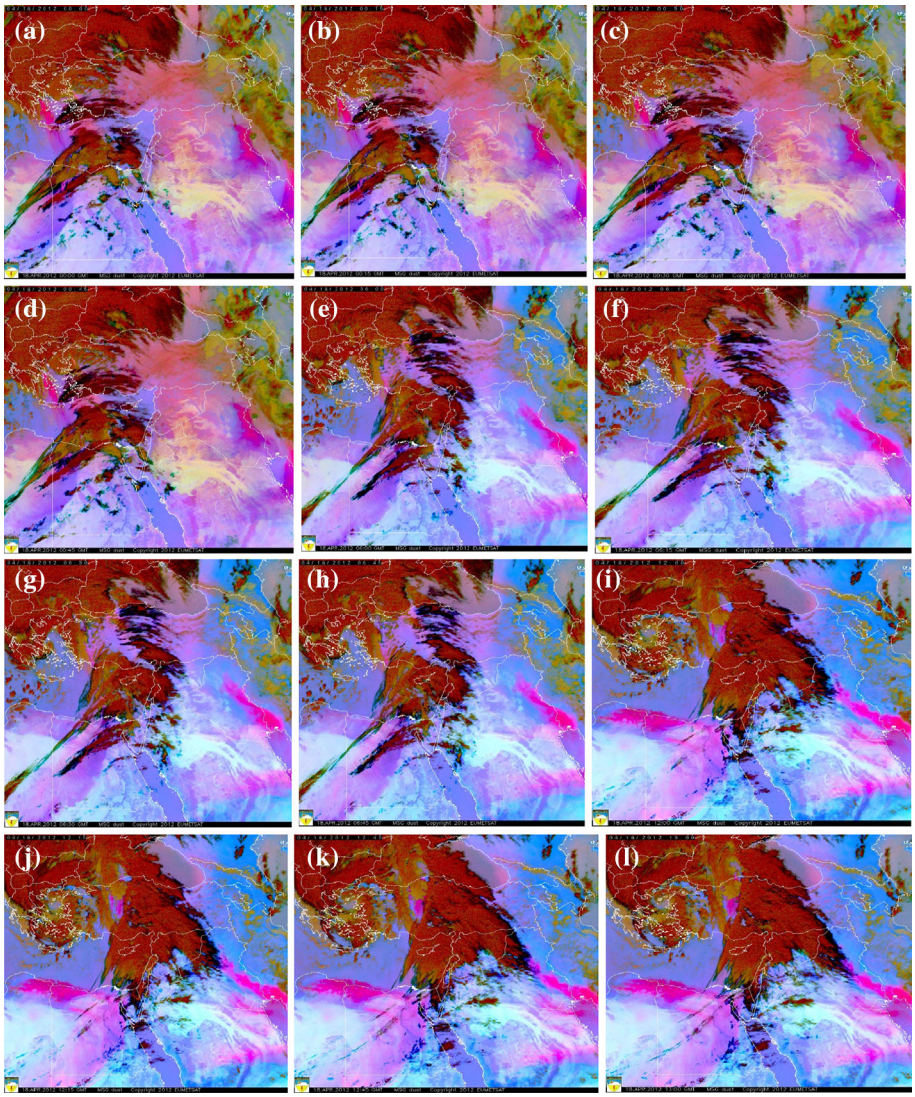

Fig. 9 Images for MSG dust satellite on April 18, 2012; **a** 0000 UTC, **b** 0015 UTC, **c** 0030 UTC, **d** 0045 UTC, **e** 0600 UTC, **f** 0615 UTC, **g** 0630 UTC, **h** 0645 UTC, **i** 1200 UTC, **j** 1215 UTC, **k** 1245 UTC, **l** 1300 UTC. *Source* Turkish State Meteorological Service, MGM

4.4 Upper air sounding plots

The conditions on April 18, 2012, 0000 UTC are shown in the skew-T/log-P diagram received from the western and inner region of radiosonde stations in Turkey (Fig. 10). The speeds of 60 knots are reached between 143 and 295 hPa in Samsun; additionally, its maximum speed was 95 knots from 280° at 243 hPa. As given in Fig. 10a, vertical totals was 30.50. The wind speed of Istanbul was 60 knots between 323 hPa to 117 hPa and 96.7 hPa to 97.0 hPa; at the same time, the maximum speed of 115 knots have been

reached at 217 hPa from 245°. Vertical totals was 33.10, and total totals was 50.20 (Fig. 10b). Wind passed with 60 knots values occurred between altitude 126 hPa and 303 hPa in Ankara region, and the maximum wind of 115 knots was reached from 265° at 187 hPa. Vertical totals was 29.30 (Fig. 10c). The maximum wind speed of 124 knots was reached from 245° at 199 hPa in İzmir. Sixty knots speed took place between 111 and 768 hPa; total totals was 39.60 (Fig. 10d). In Isparta, wind reached the maximum speed as 129 knots at 182 hPa from 265° (Fig. 10e). Between 123 and 342 hPa, speed was measured as 60 knots, and the wind reached a maximum speed of 125 knots from 280° at 213 hPa; vertical totals was 29.502 over Adana which is shown in Fig. 10f.

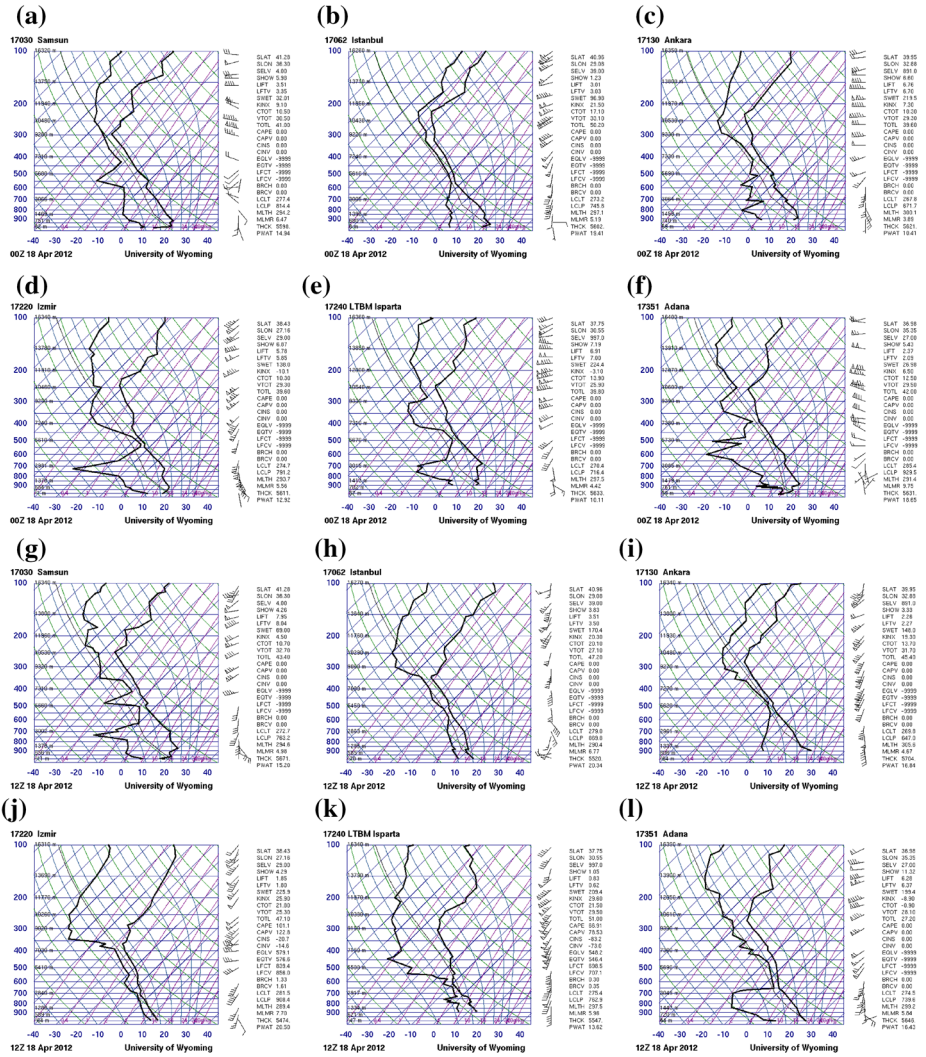

Fig. 10 Skew-T diagrams on April 18, 2012, 0000 UTC; **a** Samsun, **b** İstanbul, **c** Ankara, **d** İzmir, **e** Isparta, **f** Adana; on April 18, 2012, 1200 UTC; **g** Samsun, **h** in İstanbul, **i** Ankara, **j** İzmir, **k** Isparta, **l** Adana *Source* http://weathefr.uwyo.edu/upperair/europe.html

In Fig. 10 are shown the skew-T diagrams received from the radiosonde stations in the west and interior part of Turkey on April 18, 2012, 1200 UTC. Fig. 10g to l displays the upright atmospheric structure of different cities. In Samsun, between 358 and 161 hPa, wind speed was measured as 60 knots, and it reached the maximum value of 90 knots at 167 hPa from 245° with vertical totals 32.70 (Fig. 10g). In İstanbul, wind was 60 knots from 514 to 130 hPa, and the speed reached 140 knots at 81 hPa with 195° with vertical totals 27.10 (Fig. 10h). Sixty knots of wind occurred between 652 and 163 hPa in Ankara. A maximum wind speed of 88 knots was reached from 205° at 280 hPa with vertical totals 31.70 (Fig. 10i). The maximum wind speed of 220° has extended 67 knots at the level 170 hPa (Fig. 10j). Wind speed is 60 knots from 581 to 173 hPa in Isparta, and the maximum wind speed is 128 knots at 270 hPa from 215°. K index is 29.60; vertical totals is 29.50, and total totals is 51.00 (Fig. 10k). In Adana, 60 knots were measured between 472 and 150 hPa. The highest value is 103 knots at 160 hPa from 250°; vertical totals is 28.10 (Fig. 10l).

5 Evaluation of upper air and wind field

5.1 Evaluation of upper air sounding plots

The comparison of meteorological variables between April 18, 2012, 1200 UTC and 42-year period from 1970 to 2011 revealed highly distinct atmospheric conditions. The mean and minimum geopotential height anomalies are calculated as −179.2 m and −22 m correspondingly at 850 hPa on IST/AHL (Tables 1, 2). The anomalies of mean geopotential heights of 700 hPa, 500 hPa and 300 hPa relatively are observed with the negative values of −157.9 m, −138.4 m and −86.5 m. The mean geopotentials are measured with positive anomalies upper altitudes from 200 to 10 hPa although anomalies of minimum height started to increase entire levels after 700 hPa up to 10 hPa. Mean geopotential heights have developed dramatically from 100 hPa to upper level of 10 hPa as 112.2, 69.5, 62.4, 44.7 and 14.1 m correspondingly. When we looked for the mean temperature, it continues to rise vertically up to 6 km from 850 to 100 hPa and then it cooled after 50 hPa (approximately 20 km).

The mean wind became stronger (almost double) at layer between 850 and 700 hPa, and it lost its power on upper altitudes. Wind speed anomaly is computed as 16.3 knots at 850 hPa. Negative anomalies of mean wind speed expanded such as −22.2 knots, −25.9 knots and −40.7 knots at higher altitudes. The mean humidity increased from surface to approximately 5 km so that the huge moisture added to atmosphere at 500 hPa around 26%. Humidity of elevated altitudes is dropped gradually; as a result of enormous moisture in the temperature and strong winds, the cyclone gained strength to move toward the inner areas of Turkey. The conditions mentioned above are revealing that the weather conditions were conducive for enormous storm.

5.2 Evaluation of the wind field for Istanbul Atatürk Airport

Istanbul is located at northwestern part of Turkey. We obtained the observed data for the recorded period of 1970–2012 from a wide range of Istanbul meteorological stations. According to previous research, the extreme storm values were documented on February

26, 1973, from the SSW direction of 82.4 knots and on January 9, 1975, from the NNW direction of 76.6 knots in Şile region, Istanbul.

Atatürk International Airport is the largest airport of Turkey located toward the southwest of Istanbul on European side. The airport has a modern passenger terminal, which spreads 10000 square meters and has a height of 49.75 m above mean sea level. The airport has three varied landing fields over approximately 4 km radius area (Fig. 11). The wind speed information is recorded with four distinct wind masts at 10-m altitude via Automated Weather Observing System (AWOS) (Fig. 11). This information is recorded by four different wind masts, which are represented with 35R, 17L, 05 and 23. Wind masts of Atatürk Airport have used Vaisala WAA151 (Vaisala 2011)-type anemometers which have accuracy ±0.19 m/s for wind speed and ±2.8° for wind direction. Other meteorological parameters are measured by Vaisala brand AWOS.

The highest pressure value (in minutes) on April 18, 2012, is 999.76 hPa between 0000 UTC and 0107 UTC in 17 min, and the lowest pressure values are measured at 0928 UTC, 0929 UTC and 0931 UTC, respectively (Fig. 12a). The highest temperature during the day is measured as 25.5 °C at 0936, 0937 and 0938 UTC; the lowest air temperature is achieved in 8 min from 2231 UTC to 2240 UTC (Fig. 12b).

The maximum wind speed is obtained in 2-min interval during 24-h period for four wind masts of IST/AHL in Fig. 12c. The 35R wind mast reached 57.4 knots speed at 1011 UTC from 220°. Other wind masts reached the greatest values as 53.1 knots at 1012 UTC, 49.6 knots at 1011 UTC and 51.4 knots at 1014 UTC for 17L, 05 and 23, respectively (it is displayed by the red dashed oval shape in Fig. 12c). In addition to that, at the beginning of the day, the maximum speed recorded is 6.4 knots at 0952 UTC, 6.8 knots at 0826 UTC, 5.6 knots at 0953 UTC and 3.9 knots at 0957 UTC over the four wind masts 35R, 17L, 05 and 23, respectively.

The wind speed in IST/AHL is raised during the passage of cold front, which is part of occlusion front of a low-pressure system with 988 hPa centered on Aegean Sea and caused wind shear at the surface. Cold front and occlusion front on the northern Aegean Sea

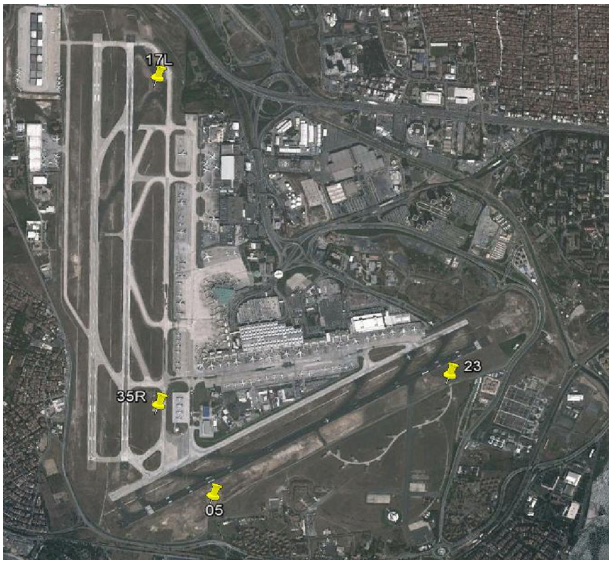

Fig. 11 Location of İstanbul Atatürk Airport (IST) landing fields and 4 different wind towers represented with 35R, 17L, 05 and 23. *Source* http://maps.google.com

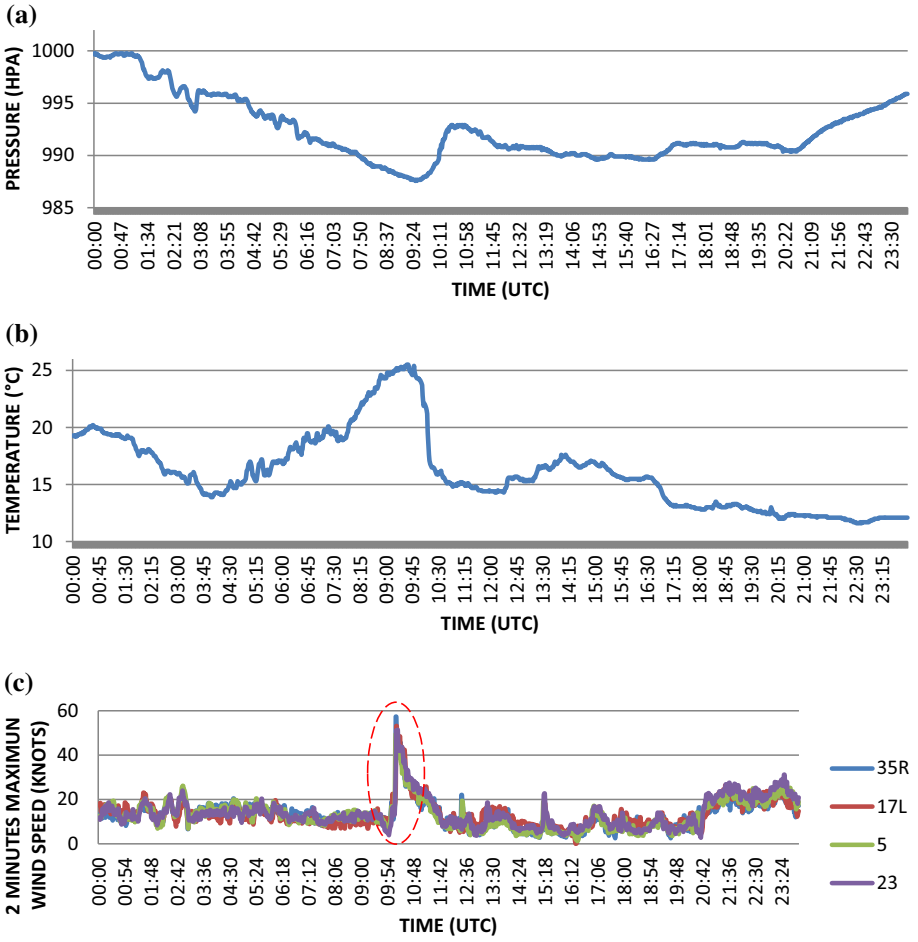

Fig. 12 Variation of **a** pressure (hPa), **b** temperature (°C) and, **c** the maximum wind speed (knots) for 24 h on April 18, 2012, in Atatürk Airport

through the passage over Istanbul are shown as MSG infrared images in Fig. 13a–f and MSG visible images in Fig. 13g–l. Satellite images imply the spiral vortex area circling through the low-pressure center.

Radar of Çatalca, Istanbul, has 375 m height, and it is located at the northwest of IST/AHL from about 317° and approximately 56 km far away from the airport. The images of Plan Position Indicator (PPI) display and Volume Velocity Processing (VVP) of radar are shown in Fig. 14a, b belonging to stormy day at 1012 UTC. VVP image (maximum distance 30 km) displayed the maximum wind speed values, for instance 105 knots from the southeast at 3–4 km height between 0915 UTC and 1010 UTC, 50 knots from southeast at 4–5 km altitudes, 70 knots from southwest at 5–6 km and 120 knots from the south at 6–7 km heights.

The highest values are obtained from 1000 UTC to 1030 UTC so that the meteorological parameters are explored in detail in this interval. The METAR weather report of Atatürk Airport has shown total coverage of 5 out of 8 on 0950 UTC, 1020 UTC and 1050 UTC. There are no unusual weather events for three observations on stormy day, while the sky was covered with 3/8 cumulus at 3500 feet and 5/8 altocumulus at 10,000 feet.

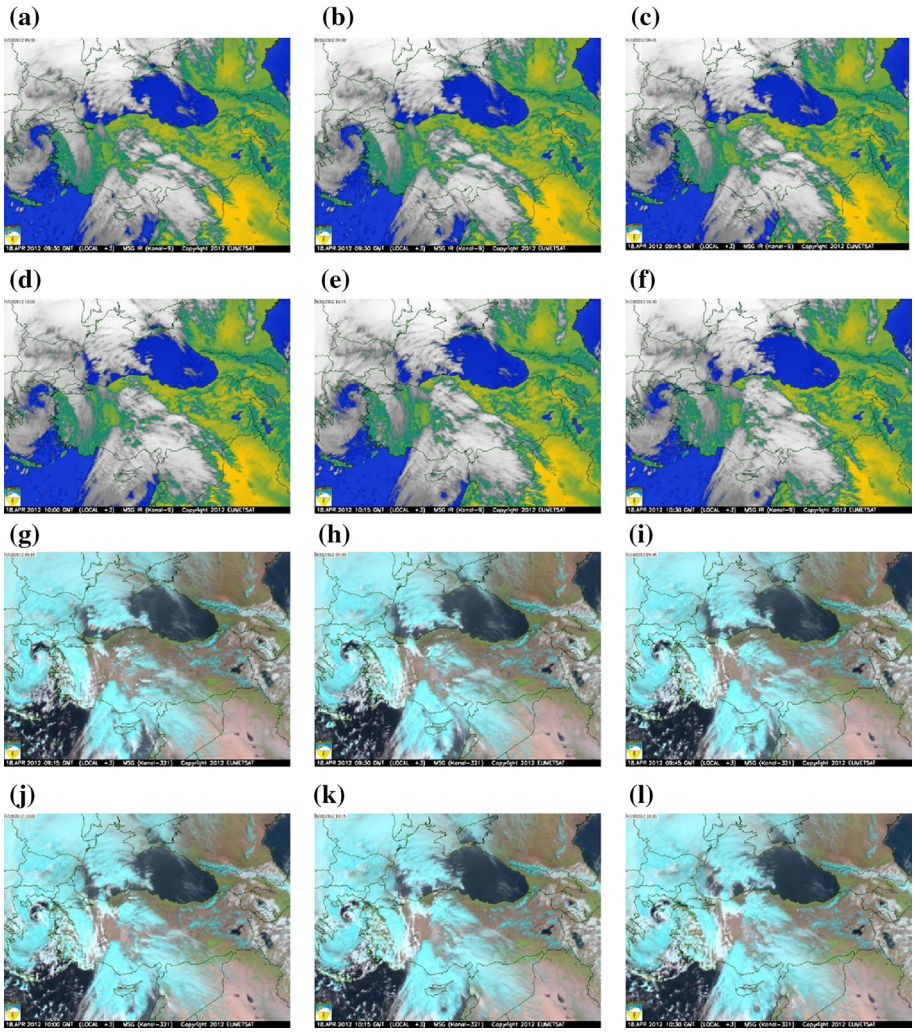

Fig. 13 MSG infrared images of stormy day; **a** 0915 UTC, **b** 0930 UTC, **c** 0945 UTC, **d** 1000 UTC, **e** 1015 UTC, **f** 1030 UTC; and MSG visible images of stormy day; **g** 0915 UTC, **h** 0930 UTC, **i** 0945 UTC, **j** 1000 UTC, **k** 1015 UTC and **l** 1030 UTC. *Source* MGM

Wind speed began to rise after 1000 UTC on four wind masts, and the highest value of 35R was measured as 57.4 knots from 220° at 1011 UTC. Other wind masts of 17L, 05 and 23, respectively, have reached maximum values as 53.1 knots at 1012 UTC, 49.6 knots at 1011 UTC and 51.4 knots at 1014 UTC (Fig. 15a).

Figure 15b shows 2-min maximum wind direction from 1000 to 1030 UTC on stormy day at Atatürk Airports, and the wind direction varies between 194° and 252°. Moisture at the beginning of storm at 1000 UTC was 29% in air, and then, it extended to 62% until 1030 UTC in 30-min period (Fig. 15c). Humidity of storm has increased gradually such as 3% at 1011 UTC to 6% at 1012 UTC. The pressure on 1000 UTC is 988.86 hPa in 30 min and it increased to 992.71 hPa consequently at the end of the period. The variation of pressure in 30-min period is around 3.85 hPa (Fig. 15d).

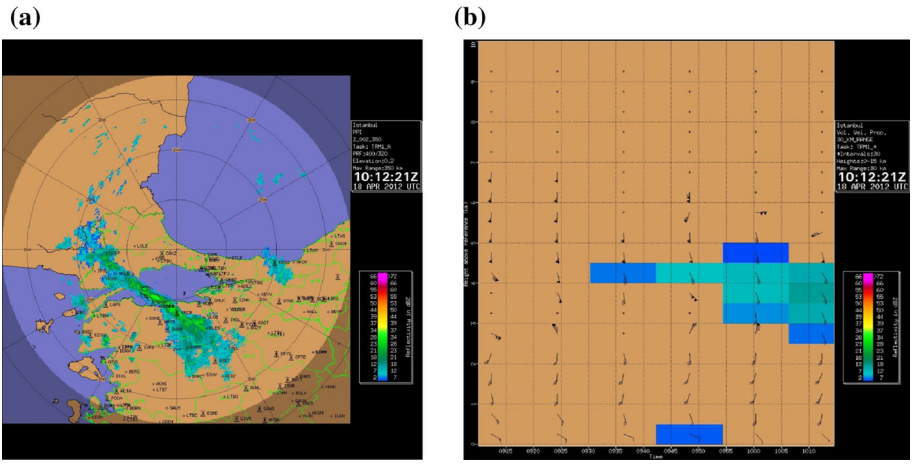

Fig. 14 Radar images of Istanbul on April 18, 2012, 1012 UTC; **a** Plan Position Indicator (PPI) display, **b** Volume Velocity Processing (VVP). *Source* MGM

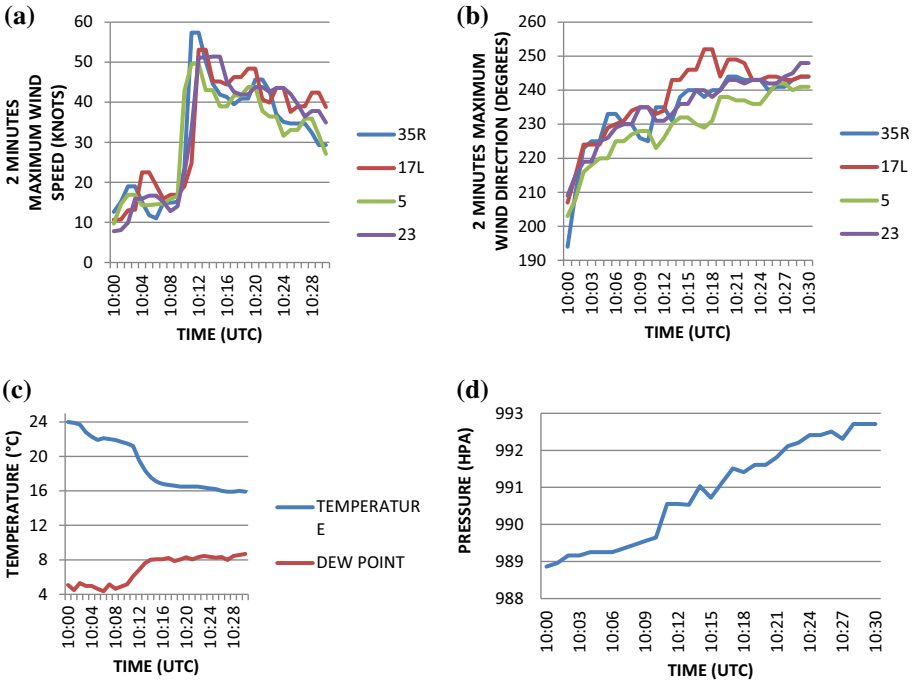

Fig. 15 Temporal variation on April 18, 2012, from 1000 to 1030 UTC in Atatürk Airport, **a** the maximum wind speed (knots), **b** the maximum wind direction (°), **c** environmental temperature and dew point–temperature (^{0} C), **d** pressure (hPa)

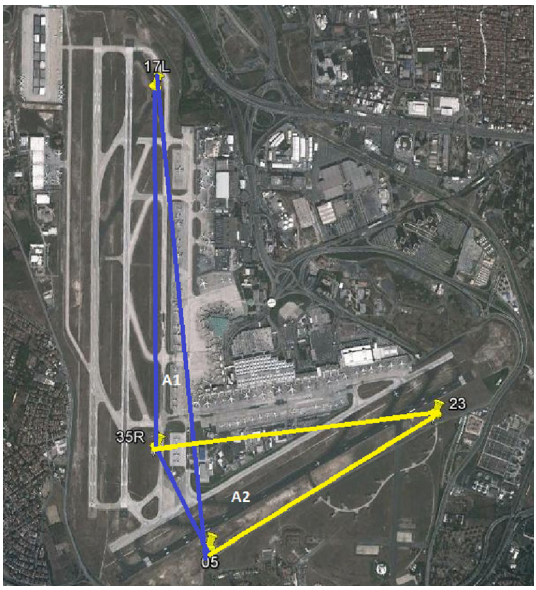

Fig. 16 A1 and A2 domains in Atatürk Airport. *Source* http://maps.google.com

6 Computing of divergence and vorticity

Coordinate of four different wind observing masts, which are located at each head of landing fields, is used to compute the distance from each other. Four winds observing masts are named as 35R, 17L, 05 and 23. The origin of *x*-axis and *y*-axis is found by using wind masts 05 and 17L located at the head of airfields, and other two wind masts namely 35R and 23 remained positive about the direction of the coordinate system (Figs. 11 and 16). The mean divergence and vorticity are computed from the area between these four wind observing masts by using 2-min maximum wind speed, 2-min average wind speed and instantaneous measured wind speed from four wind masts stated in the head of landing fields. The calculations were made in the direction of rotation counterclockwise.

$$\oint \boldsymbol{U} \cdot \mathrm{d}\boldsymbol{l} = \iint_{A} (\nabla \times \boldsymbol{U}) \times \boldsymbol{n} \mathrm{d}A \tag{1}$$

$$\oint u\mathrm{d}x + v\mathrm{d}y = \int\int \frac{\partial v}{\partial \mathrm{x}} - \frac{\partial u}{\partial \mathrm{y}} \mathrm{d}x\mathrm{d}y \tag{2}$$

Equations (1) and (2) show the finite-dimensional shapes of the two-dimensional form of Stokes theorem, which connects vorticity to circulation (Holton 2004). $\boldsymbol{U}$ is three-dimensional velocity vector; **l**, a line delimited surface; ∇, nabla operator; **A**, delimited area by the contour of the area; **n**, unit vector normal to field element (it is positive according to the right-hand rule); **u**, *x*-component of wind velocity (to the east); and **v**, *y*-component of the velocity (to the north). Stokes theorem proposes that the surface integral of the curl of a function over any surface bounded by a closed path is equal to the line integral of a particular vector function around that path (named after Sir G. Stokes). For this reason, the average normal component of vorticity is calculated for a finite field by dividing circulation to area. The formula is expressed in Eq. 3.

$$\zeta = \frac{1}{\text{AREA}} \oint (u\text{dx} + v\text{dy}) \tag{3}$$

In a similar way, Eq. (5) as a two-dimensional form of divergence is extracted from Eq. (4) by using divergence theorem (Holton 2004), where **B** is the vector field; **V** is volume; **A** is closed surface; and **n** is a normal unit vector to **dA** area element. As a result, the divergence is expressed in Eq. 6.

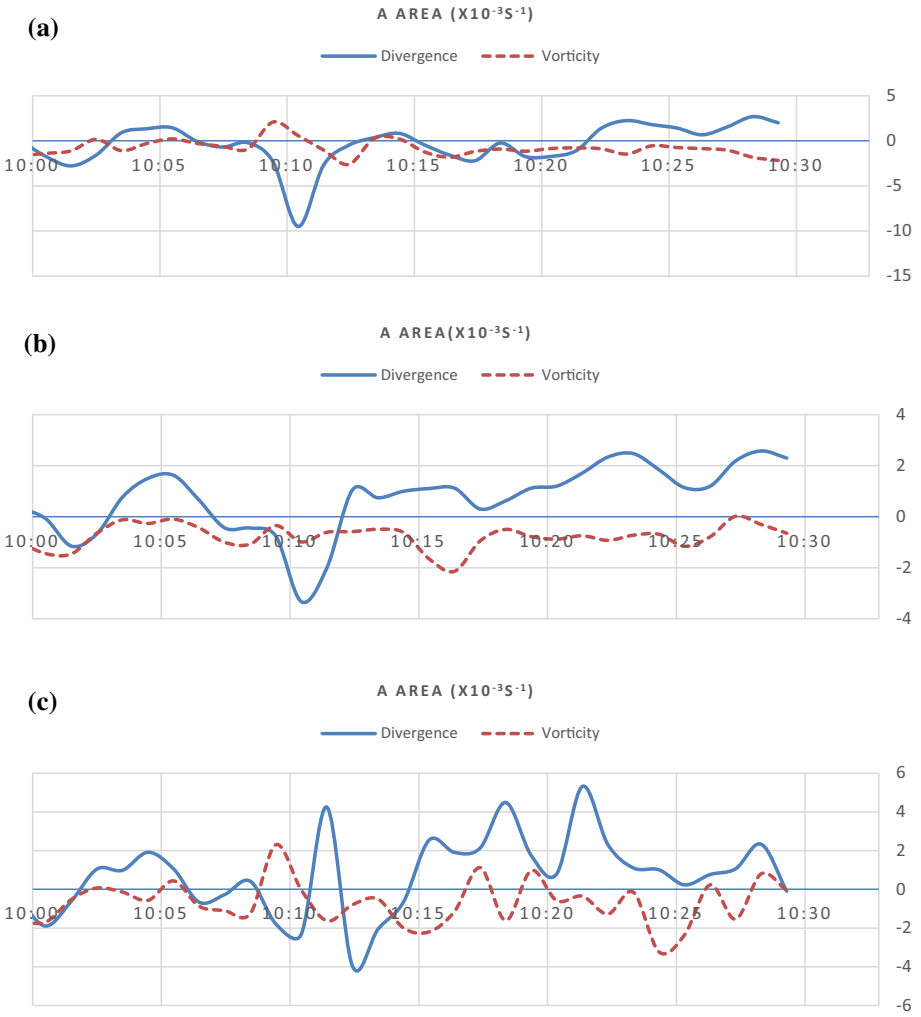

Fig. 17 Temporal variation of average divergence and vorticity ($\times 10^{-3}$ s^{-1}) values that belong to area "A" in Atatürk Airport on April 18, 2012, 1000 UTC–1030 UTC obtained by using **a** maximum wind speed, **b** average wind speed and **c** instant wind speed in 2 min

$$\oint_A \mathbf{B} \cdot \mathbf{n} dA = \iint_V \mathbf{V} \cdot \mathbf{B} dV \tag{4}$$

$$\oint (u\mathrm{dx} - v\mathrm{dy}) = \iint \left(\frac{\partial v}{\partial \mathrm{x}} + \frac{\partial u}{\partial \mathrm{y}} \right) \mathrm{dxdy} \tag{5}$$

$$\mathrm{Div} = \frac{1}{\mathrm{AREA}} \oint (u\mathrm{dy} - v\mathrm{dx}) \tag{6}$$

Average divergence and average vorticity are computed according to measurements received by four observation masts and for the area (trapezoidal area) stated among them, namely 17L, 35R, 05 and 23 (Figs. 11 and 16). The comparisons of the average divergence and vorticity values are made from 1000 UTC to 1030 UTC by using 2-min maximum wind speed; 2-min average wind speed and instantaneous wind is shown in Fig. 17a–c.

The maximum wind speed is 57.4 knots at 1011 UTC at 35R mast by using 2-min interval dataset, and the maximum divergence and vorticity are calculated, which are shown in Fig. 17a. Figure 17b shows average vorticity and divergence values, which are changing from 1000 UTC to 1030 UTC by using average wind speed measured in 2-min interval. These data are used to compute divergence and vorticity, and their maximum values are shown in third row of Table 4. Same calculation was repeated with instant wind speed data (Fig. 17c) to find divergence and vorticity values, and the maximums are presented in the fourth row of Table 4.

The above-average divergence and vorticity calculations are done for the area stated among four observation masts, so that this approach is proposed as a trapezoid for very narrow field. The second calculation for divergence and vorticity is made for two triangle fields, which are named as A1 area and A2 area. The first triangle is positioned between 35R, 17L and 05 wind masts, and the other one is placed on 35R, 05 and 23 as A2 area (Fig. 16). The comparison of vorticity and divergence is presented in Fig. 18a–l for 2-min maximum, average and instant wind speeds separately.

The A1 area received 21.22528×10^{-3} s^{-1} divergence at 1010 UTC, which is calculated by using 2-min maximum wind speeds during 30-min period, and then, 1 min later 1011 UTC, the maximum convergence value is -34.4287×10^{-3} s^{-1} (Fig. 18a). The value of vorticity at 1010 UTC reached the maximum value 14.65287×10^{-3} s^{-1} in the 30-min period. At the same time period, maximum convergence in A2 area is -11.194×10^{-3} s^{-1} at 1011 UTC and the maximum vorticity at 1010 UTC is 11.33702×10^{-3} s^{-1} (Fig. 18b).

The comparisons of divergence and vorticity by computing 2-min maximum wind speed are displayed for 30-min duration in Fig. 18c, d. When we examined the figures, it seems that the passage of cold front caused strong surface gusts effectively in A1 area. This area

Table 4 Maximum divergence and vorticity values of area "A" during 30-min period

	Maximum divergence ($\times 10^{-3}$ s^{-1})	Maximum vorticity ($\times 10^{-3}$ s^{-1})
Maximum wind speed	−9.50375	0.562362
Average wind speed	−2.95917	−1.21781
Instantaneous wind speed	5.316882	−0.35302

Fig. 18 Comparison of average divergence ($\times 10^{-3}$ s^{-1}) and average vorticity values that belong to A1 area and A2 area of Atatürk Airport on April 18, 2012, 1000 UTC–1030 UTC obtained by using maximum wind speed in 2-min interval; **a** A1 area, **b** A2 area, **c** divergence and **d** vorticity, by using average wind speed in 2-min interval; **e** A1 area, **f** A2 area, **g** divergence and **h** vorticity, by using instantaneous wind speed in 2-min interval; **i** A1 area, **j** A2 area, **k** divergence and **l** vorticity

provides more contributions on average divergence and vorticity values on stormy day in 30-min period.

Divergence is 5.972814×10^{-3} s^{-1} at 1010 UTC in A1 area. At 1012 UTC, largest convergence is -12.2309×10^{-3} s^{-1} by computing average wind speed with 2-min interval; besides, vorticity is -5.91227×10^{-3} s^{-1} at 1012 UTC in 30-min period (Fig. 18e). The maximum convergence and vorticity are -3.58789×10^{-3} s^{-1} at 1011 UTC and -4.63482×10^{-3} s^{-1} at 1012 UTC, respectively, in A2 area (Fig. 18f).

Another comparison for divergence and vorticity is made on stormy day by using 2-min average wind speed, which is shown in Fig. 18g, h. When Fig. 18g, h are examined, average divergence and vorticity in A1 area are higher than that in A2 area. So that A1 area made more contributions on these values.

When we examined the instant wind speed in A1 area for the same time period, the maximum divergence and convergence are $22.8914 \times 10^{-3}\ s^{-1}$ at 1010 UTC and $-30.3535 \times 10^{-3}\ s^{-1}$ at 1014 UTC separately. The highest vorticity is $19.09073 \times 10^{-3}\ s^{-1}$ at 1010 UTC in A1 area (Fig. 18i). While A1 area is shown in Fig. 18i, A2 area is shown in Fig. 18j by using instant wind speed data. At 1010 UTC, maximum convergence and vorticity are $-8.44728 \times 10^{-3}\ s^{-1}$ and $12.00187 \times 10^{-3}\ s^{-1}$ (Fig. 18j). The evaluation of average divergence and vorticity for A1 and A2 areas is shown in Fig. 18k, l. The average values of A1 area are higher than that of A2 area, so that the contribution of divergence and vorticity on stormy day seems to be higher in A2 area on April 18, 2012, 1000 UTC—1030 UTC.

7 Discussion and results

The initial conditions of cyclone started on UK, Sweden, west and northwestern parts of Mediterranean region. Later days the weather system moved to Mediterranean region, which overheated the system from the bottom, depending upon the result from the activity of the thermodynamic changes; it loses its place in a wider area (into the area of Italy, France, Spain, Algeria and France), and it left −25 °C isotherm that made a cutoff from northern Europe on April 16, 2012, 1800 UTC. The jet stream started from the North Atlantic, and it descended to Spain and central Mediterranean as a result the low-pressure system moved to the south. Besides that, on April 17, 2012, 1200 UTC, the weather system was affected by two other jet streams which were passing over North Africa.

The system had progressed toward the east and northeast, and the cutoff isotherm of −25 °C protected its presence over Italy, Greece and Libya on April 18, 2012, 0600 UTC. Mediterranean Sea is essential source for energy of weather system in the region. When the system lost its energy, it was replaced with the isotherm of −25 °C over Turkey, Libya and Italy at 1200 UTC. The isotherm of −20 °C moved from the western region of Turkey and the northeast of Cyprus Island to Greece at 1800 UTC, and on April 19, 2012, 0000 UTC, the system enlarged toward the interior regions of Turkey.

The comparison is made for 40-year data (1970–2011) of April and the result of Temp diagram of April 18, 2012, 1200 UTC in İstanbul; the average and minimum height of stormy day at 850 hPa are lower than in the comparison period, −179.2 and −22, respectively. The average geopotential heights of April 18, 2012, at 700 hPa, 500 hPa and 300 hPa altitudes are lower than the mean values of 40 years so that anomalies are calculated as −157.9 m, −138.4 m and −86.5 m separately. The A1 area of Atatürk International Airport is designed to compute divergence, convergence and vorticity from 1000 UTC to 1030 UTC by using 2-min maximum wind speed. The divergence and convergence results are obtained as $21.22528 \times 10^{-3}\ s^{-1}$ at 1010 UTC and as maximum value $-34.4287 \times 10^{-3}\ s^{-1}$ at 1011 UTC separately. The maximum vorticity value in the 30-min period between 1000 and 1030 UTC is calculated as $14.65287 \times 10^{-3}\ s^{-1}$ at 1010 UTC.

Similar results are found for A2 area so that the maximum convergence and vorticity are $-11{,}194 \times 10^{-3}\ s^{-1}$ value at 1011 UTC and $11.33702 \times 10^{-3}\ s^{-1}$ at 1010 UTC. The

2-min maximum wind speed is used to calculate average divergence and vorticity to compare area of A1 and A2 on April 18, 2012 at 1010 UTC. The cold front passage became more effective in the next 30-min period so that the surface gust is observed in the area of A1. Therefore, we could suggest that the contribution average convergence and vorticity values of A1 area are more than that of A2 area in the computed total area.

The stormy day caused very extreme and severe damages on west, southwest and northwest region of Turkey as reported by government agencies and media. According to information from Turkish State Meteorological Service, the forest fires started due to the overthrow of power lines in Amasra and Kurucas city. In many cities, provincial centers, districts and villages, it was reported that the roofs of some buildings and greenhouse farms were thrown far; trees and billboards were overturned; many branches of trees were broken and blown off to another places; the traffic signs were removed and damaged. Many people and animals were injured because of roofs damages and flying of the billboards. The energy and communication lines of some settlements were damaged as a result short-term interruptions occurred. The storm caused disruption to land, sea and air traffic. Dust storm resulted in decline of the visibility and muddy rain precipitated in some cities. The wind speed increased to 65 knots at times in different places of Cihanbeyli and Konya, and then, the high speed formed dust storm that caused a sudden fall of the visibility, and therefore, the disruptions occurred in land transportation. Two people died due to a chain traffic accident caused by dust storm at Cihanbeyli and Konya highway.

Wind speeds reach 50 knots in total 5 min and caused the diversion of aircrafts from the Atatürk Airport where they were going to land. In addition, 34 people were injured: three of them heavily; 350 roofs were blown off, and 118 trees were cut down across Istanbul. The bridges which connect European continent to Asian continent, namely Bosporus and Fatih Sultan Mehmet, were closed to vehicle traffic. Dusts hurtling incident was reported in Atatürk and Sabiha Gokcen Airports in this 5-min period of short time. In Sabiha Gokcen Airport which is located in Asian continent, dust storm which occurred at 1020 UTC, 1028 UTC and 1050 UTC caused gust with maximum of 59 knots wind speed. The maximum value of wind speed had reached 57 knots on 1032 UTC at Istanbul Samandıra Army Air Base in Asian continent, and at the same time, dust storm was reported 1 km dominant horizontal and vertical viewing of Army Air Base.

The fire started in the forest areas of Mengen Province of Bolu and Safranbolu Province of Karabük, and due to the influence of the storm, the fire grew rapidly and 25-acre woodland burned in Mengen region. As a result of the fire, five homes burned down completely that occurred in the village of Çökeler of Bolu. Three people died due to fly of the roof tiles in Kırıkkale, to fall off a roof in Bolu, and to overthrow of the motorcycle in Denizli.

Aviation industry, International Civil Aviation Organization (ICAO) and the World Meteorological Organization (WMO) agencies should design future airports according to short-term microscale hazardous and extreme weather events due to the global warming. The aviation industry could enhance new innovative strategy of microscale meteorological observation system that can evaluate the extreme and dangerous weather events in short time. Number of meteorological variables can be increased by additional measurement instruments or observing systems to evaluate more accurate weather extremes, hazards and prediction in airports. This also could provide better understanding of microscale atmospheric phenomena.

In future studies, the Weather Research and Forecasting (WRF) Model can be used for a comprehensive research to simulate such extreme cyclones.

Acknowledgement We like to appreciate the Branch Office of Software and Hardware of Turkish State Meteorological Service for their meteorological data support. In addition to that, we thank the Meteorology Office of Atatürk International Airport for their help in obtaining the meteorological data belonging to Atatürk International Airport. We are thankful to ECMWF for reanalysis datasets and GrADS package to draw figures.

References

Alpert P, Ziv B (1989) The Sharav cyclone: observation and some theoretical considerations. J Geophys Res 94:18495–18514

Alpert P, Neeman BU, Shay-El Y (1990a) Climatological analysis of Mediterranean cyclones using ECMWF data. Tellus A 42:65–77

Alpert P, Neeman BU, Shay-El Y (1990b) Intermonthly variability of cyclone tracks in the Mediterranean. J Clim 3:1474–1478

Bartzokas A, Lolis CJ, Metaxas DA (2002) A study on the intra-annual variation and the spatial distribution of the precipitation amount and duration over Greece on a 10 day basis. Int J Climatol 23:207–222

Buzzi A, Tibaldi S (1978) Cyclogenesis in the lee of the Alps: a case study. Q J R Meteorol Soc 104:271–287

Cavicchia L, Storch H, Gualdi S (2014) A long-term climatology of medicanes. Clim Dyn 43:1183–1195. doi:10.1007/s00382-013-1893-7

Deniz A, Karaca M (1995) Analysis of cyclone tracks effecting Turkey. J İstanb Tech Univ 53:59–66 **(in Turkish)**

Deniz, A, Karaca, M, Borhan, Y, (1997) A climatological study on the relationship between cyclone paths and air pollutants in Turkey. In: Air quality management at urban, regional and global scales environmental research forum, vol 7–8, pp 360–366

Deniz A, Özdemir ET, Sezen İ, Coşkun M (2012) Investigations of storms in the region of Marmara in Turkey. Theor Appl Climatol. doi:10.1007/s00704-012-0715-x

Egger J, Alpert P, Tafferner A, Ziv B (1995) Numerical experiments on the genesis of Sharav cyclones: idealized simulation. Tellus 47A:162–174

Flocas, HA, Kouroutzoglou, J, Keay, K, Hatzaki, M (2009) Cyclonic tracks over eastern mediterranean in the present climate. In: International conference on environmental science and technology Chania, Crete, Greece

Goyette S (2011) Synoptic conditions of extreme windstorms over Switzerland in a changing climate. Clim Dyn 36:845–866

Grumm RH (2010) The devastating Western European winter storm 27–28 February 2010. Weather Case Studies for Central Pennsylvania. http://nws.met.psu.edu/severe/2010/28Feb2010.pdf

Grumm RH, Lambert B (2010) The convective high wind event of 16 April 2010. Weather Case Studies for Central Pennsylvania. http://nws.met.psu.edu/severe/2010/16Apr2010.pdf

Hewson TD, Neu U (2012) Cyclones, windstorms and the IMILAST project. Tellus 67:1–33

Holton JR (2004) An introduction to dynamic meteorology. Elsevier Academic Press, Oxford, pp 46, 92, 93, 499

Hruska C (2006) Case study of a downslope windstorm April 23 1999 wasatch range. J Univ Wis Atmos Ocean Sci Dep. http://www.aos.wisc.edu/uwaosjournal/Volume1/AOS453/FCS_Hruska.pdf

http://maps.google.com. Received date: 23 November 2012

http://weathefr.uwyo.edu/upperair/europe.html. Received date: 9 December 2012

Kalnay E, Kanamitsu M, Kistler R, Collins W, Deaven D, Gandin L et al (1996) The NCEP/NCAR 40 year reanalysis project bull. Am Meteor Soc 77:437–471

Karaca M, Deniz A, Tayanç M (2000) Cyclone track variability over Turkey in association with regional climate. Int J Climatol 20:1225–1236

Koç T, Türkeş M, Çalışkan V (2005a) Geographical analysis of formation and effects of Çanakkale snow storm in Jan 2004. Coğrafi Bilgi Sistemleri Sempozyumu İzmir Ege University (**in Turkish**)

Koç T, Türkeş M, Çalışkan V, Sarışın F, İrdem C, Çavuş C, et al (2005b) Local scale evaluation of social effects by Çanakkale snow storm disaster at 22–25 January 2004. National Geography Congress İstanbul (**in Turkish**)

Kömüşcü AÜ, Çelik S, Ceylan A (2011) Rainfall analysis of the flood event that occurred in Marmara Region on 8–12 September 2009. Coğrafi Bilimler Dergisi 9(2):209–220 **(in Turkish)**

Lionello P, CMCC (Centro euroMediterraneo peri Cambiamenti Climatici) (2012) The climate of the mediterranean region from the past to the future, Elsevier, ISBN: 978-0-12-416042-2, pp 502

Lionello P, Malanbotte-Rizzoli P, Boscolo R (eds.) (2006) Mediterranean climate variability, developments in earth and environmental sciences 4. Elsevier, Radarweg 29, Amsterdam, The Netherlands

Mascatello A, Miglietta MM, Rotunno R (2008) Numerical analysis of mediterranean hurricane over southeastern Italy. Mon Weather Rev 136:4373–4397

Saaroni H, Ziv B, Bitan A, Alpert P (1997) Easterly wind storms over Israel. Theor Appl Climatol 59:61–77

Şahin AD (2002) Hourly wind velocity exceedence maps of Turkey. Energ Convers Manag 44:549–557

Sirdas S (2005) Daily wind speed harmonic analysis for Marmara region in Turkey. Energ Convers Manag 46:1267–1277

Sirdas S, Ross RS, Krishnamurti TN, Chakraborty A (2007) Evaluation of the FSU synthetic superensemble performance for seasonal Forecasts over the Euro-Mediterranean region. TellusA 59(1):50–70

Stuart NA, Grumm RH (2006) Using wind anomalies to forecast east coast winter storms. Weather Forecasting 21:952–968

Tayanç M, Karaca M, Dalfes HN (1998) March 1997 cyclone (blizzard) over the eastern Mediterranean and Balkan region associated with blocking. Mon Weather Rev 126:3036–3047

Thorncroft CD, Flocas HA (1997) A case study of Saharan cyclogenesis. Mon Weather Rev 125:1147–1165

Toros H, Geertsema G, Cats G (2010) Evaluation of Hirlam and Harmonie precipitation forecasts for the Istanbul flash flood event of September 2009. Hirlam Newslett 56:37–46

Trigo IF, Davies TD, Bigg GR (1999) Objective climatology of cyclones in the Mediterranean region. J Clim 12:1685–1696

Trigo IF, Davies TD, Bigg GR (2000) Decline in Mediterranean rainfall caused by weakening of Mediterranean cyclones. Geophys Res Lett 27(18):2913–2916

Türkeş M (1996) Spatial and temporal analysis of annual rainfall variations in Turkey. Int J Climatol 16:1057–1076

Türkeş M (1998) Influence of geopotential heights, cyclone frequencies and Southern Oscillation on rainfall variations in Turkey. Int J Climatol 18:649–680

Türkeş M (2004) An evolution about 2004 winter and anthropogenic meteorological disasters. 2023 Monthly Journal 42:76–79

Türkeş M (2010) Climatology and meteorology. Kriter Press. pp 448–452 (**in Turkish**)

Turoğlu H (2010) Flood by precipitation occurred around Silivri-Selimpaşa coastal zone in 8–10 September 2009. In: II National flood symposium book Istanbul DSİ Genel Müdürlüğü pp 31–43 (**in Turkish**)

Unger Z (1996) Heat island intensity with different meteorological conditions in a medium-sized town: Szeged, Hungary. Theoret Appl Climatol 54:147–151

Vaisala (2011) Avimet, delivery documentation, Volume 1, system description, Chapter 3, WAA151 Anemometer and WAV151 Wind Wane (Existing from 2002)

Zhao TL, Gong SL, Zhang XY, Jaffe DA (2008) Asian dust storm influence on North American ambient PM levels: observational evidence and controlling factors. Atmos Chem Phys 8:2717–2728